Factors Affecting the Appearance of the Hump Charge Movement Component in Frog Cut Twitch Fibers

CHIU SHUEN HUI

From the Department of Physiology and Biophysics, Indiana University Medical Center, Indianapolis, Indiana 46223

ABSTRACT Charge movement was measured in frog cut twitch fibers with the double Vaseline gap technique. Five manipulations listed below were applied to investigate their effects on the hump component (I_γ) in the ON segments of TEST minus CONTROL current traces. When external Cl^- was replaced by $MeSO_3^-$ to eliminate Cl current, I_γ peaked earlier due to a few millivolts shift of the voltage dependence of I_γ kinetics in the negative direction. The Q-V plots in the TEA.Cl and TEA.$MeSO_3$ solutions were well fitted by a sum of two Boltzmann distribution functions. The more steeply voltage-dependent component (Q_γ) had a $\overline{V}$ ~6 mV more negative in the TEA.$MeSO_3$ solution than in the TEA.Cl solution. These voltage shifts were partially reversible. When creatine phosphate in the end pool solution was removed, the I_γ hump disappeared slowly over the course of 20–30 min, partly due to a suppression of Q_γ. The hump reappeared when creatine phosphate was restored. When 0.2–1.0 mM Cd^{2+} was added to the center pool solution to block inward Ca current, the I_γ hump became less prominent due to a prolongation in the time course of I_γ but not to a suppression of Q_γ. When the holding potential was changed from −90 to −120 mV, the amplitude of I_β was increased, thereby obscuring the I_γ hump. Finally, when a cut fiber was stimulated repetitively, I_γ lost its hump appearance because its time course was prolonged. In an extreme case, a 5-min resting interval was insufficient for a complete recovery of the waveform. In general, a stimulation rate of once per minute had a negligible effect on the shape of I_γ. Of the five manipulations, $MeSO_3^-$ has the least perturbation on the appearance of I_γ and is potentially a better substitute for Cl^- than SO_4^{2-} in eliminating Cl current if the appearance of the I_γ hump is to be preserved.

INTRODUCTION

In a previous paper, Hui and Chandler (1990) reported that the ON segments of TEST minus CONTROL current traces recorded from cut twitch fibers showed a hump charge movement component, I_γ, similar to that observed in intact fibers (Adrian and Peres, 1979), but different from some cut fiber traces published by other

Address reprint requests to Dr. Chiu Shuen Hui, Department of Physiology and Biophysics, Indiana University Medical Center, 635 Barnhill Drive, Indianapolis, IN 46223.

J. GEN. PHYSIOL. © The Rockefeller University Press · 0022-1295/91/08/0315/33 $2.00
Volume 98 August 1991 315–347

investigators (for the definitions of I_β, I_γ, Q_β, and Q_γ, refer to the preceding paper). Q_γ has been hypothesized to be the trigger for intracellular Ca release (Huang, 1982; Hui, 1983*a*, *b*; Vergara and Caputo, 1983) or a consequence of the release (Csernoch et al., 1989; Pizarro et al., 1990). The observation that cut fibers which did not show any I_γ hump could still release Ca (Melzer et al., 1986) challenged these hypotheses. However, it is possible that I_γ might still be present in TEST minus CONTROL current traces when it is not manifested as a hump (see the preceding paper). In any case, the altered kinetics of I_γ should be associated with an altered kinetics in Ca release, whether Q_γ is the cause or consequence of the release. It is thus of physiological interest to find out the underlying reason(s) for the difference in the manifestations of I_γ.

One possible cause for the alteration of the shape of I_γ was investigated by Hui and Chandler (1990), who showed that a substitution of external Cl^- by SO_4^{2-} led to an increase in I_β, making I_γ less prominent. The steady-state voltage distribution of Q_γ was not affected, but whether the kinetics of I_γ was affected was difficult to assess. The preceding paper (Hui, 1991) described another factor affecting the appearance of I_γ in cut fibers: when the temperature was lowered to <10°C, I_γ in the ON segments of TEST minus CONTROL current traces became very broad and, at ~ 6°C, completely lost its hump appearance. At this low temperature, the steady-state Q-V plot of the total charge contained a steeply voltage-dependent component, indicating the presence of Q_γ. Thus, I_γ was not suppressed at low temperatures in cut fibers, but was most likely obscured in the decay phase of I_β.

This paper shows five other conditions that apparently affect the appearance of I_γ. These interventions were studied because they have been used separately or jointly by various investigators in studying charge movement. These modifications would have some advantages in the measurement of charge movement and would be preferable if they had no effect on I_γ. They include the substitution of Cl^- in the center pool solution by $MeSO_3^-$ to eliminate Cl current, the removal of creatine phosphate in the end pool solution to simplify the procedure in preparing the solution, the addition of Cd^{2+} to the center pool solution to block Ca current, a shift of the holding potential to a more negative potential to reduce the amount of charge in the CONTROL trace, and an increase in the stimulation rate of the fiber to collect more data within a certain time period. It was concluded that each of the interventions affected the appearance of the I_γ hump.

METHODS

All experiments were performed on cut fibers stretched to a sarcomere length of 3.5 μm at 13–14°C. The experimental protocol and method of data analysis were similar to those used in previous papers (Chandler and Hui, 1990; Hui and Chandler, 1990). All traces presented are from single TEST sweeps. Unless otherwise specified, TEST runs in a complete sequence were taken at 1-min intervals. Solutions are given in Table I. For the experiments studying the effect of external Cd^{2+}, the phosphate buffer in the center pool solution (solution D) was replaced with PIPES (solution E) to avoid precipitation of the phosphates by Cd^{2+}. This replacement had no observable effect on either the kinetics of charge movement or the steady-state charge versus voltage distribution (unpublished observations).

The fitting of Q-V plots by a single Boltzmann distribution function or a sum of two

Boltzmann distribution functions included corrections for the charge movements in the CONTROL current trace (CONTROL charge correction) and for the charge movements in the membranes underneath the Vaseline seals (gap correction), as described in Hui and Chandler (1990) and Hui (1991). To avoid repetitive use of the phrase, the corrections will not be mentioned. When a sum of two Boltzmann distribution functions is used, $\overline{V}_\beta$, k_β, and $q_{\beta,max}/c_m$ are used to denote the Boltzmann parameters for the less steeply voltage-dependent component and $\overline{V}_\gamma$, k_γ, and $q_{\gamma,max}/c_m$ for the more steeply voltage-dependent component.

TABLE I

Solutions

Relaxing solution:

	K.glutamate	$MgSO_4$	K_2.EGTA	K_2.PIPES
A	120	1	0.1	5

End pool solutions:

	Cs.glutamate	Cs_2.CP	$MgSO_4$	Cs_2.EGTA	Cs_2.ATP	Glucose	Cs_2.PIPES
B	45.5	20	6.8	20	5.5	5	5
C	75.5	0	6.8	20	5.5	5	5

Center pool solutions:

	TEA.Cl	TEA.$MeSO_3$	RbCl	$CaCl_2$	Na_2HPO_4	NaH_2PO_4	PIPES
D	120	0	2.5	1.8	2.15	0.85	0
E	120	0	2.5	1.8	0	0	5
F	0	120	2.5	1.8	2.15	0.85	0

All concentrations are in millimolar. CP represents creatine phosphate in solution B. $MeSO_3$ represents methane sulfonate in solution F. Solutions D–F contained 1 μM tetrodotoxin. The relaxing and end pool solutions were titrated to pH 7.0 with KOH and CsOH, respectively. Center pool solutions D and F were titrated to pH 7.1 with HCl, whereas solution E was titrated to pH 7.1 with NaOH.

RESULTS

Effect of Substituting Cl^- *by* $MeSO_3^-$

Resting Cl conductance is known to be twice as large as K conductance in intact frog twitch fibers (Hodgkin and Horowicz, 1959; Hutter and Noble, 1960). To increase the membrane space constant, thereby improving spatial uniformity along the fiber during voltage clamp, SO_4^{2-} has been used to replace Cl^- in the center pool solution. However, Hui and Chandler (1990) showed that when extracellular Cl^- was completely replaced by SO_4^{2-}, the I_γ hump in the ON segments of TEST minus CONTROL current traces became less resolvable due to a threefold increase in Q_β, as estimated from fitting the Q-V plots by a sum of two Boltzmann distribution functions. Since Cl current can also be eliminated by replacing Cl^- with $MeSO_3^-$ (methane sulfonate), experiments were performed to investigate whether $MeSO_3^-$ affects I_β like SO_4^{2-}.

In the experiment of Fig. 1, the center pool segment of the fiber was bathed in a TEA.$MeSO_3$ solution immediately after saponin treatment. The $MeSO_3^-$ very effec-

tively blocked the positive pedestal in the ON segment arising from the nonlinear ionic current routinely seen with the TEA.Cl solution and actually gave rise to a small negative pedestal. In contrast to the SO_4 experiments, a prominent I_γ hump can be clearly seen in the ON segments of the traces between −66 and −45 mV. At −66 mV, the hump was very broad and had a very small magnitude. When the level of depolarization was increased, the hump became faster and had a larger amplitude, as routinely observed in intact fibers and our cut fibers. At potentials ≥ −58 mV, the peak of I_γ rose above that of I_β. At −40 and −30 mV, the kinetics of I_γ was even faster, such that the peak of I_β was buried in the rising phase of I_γ.

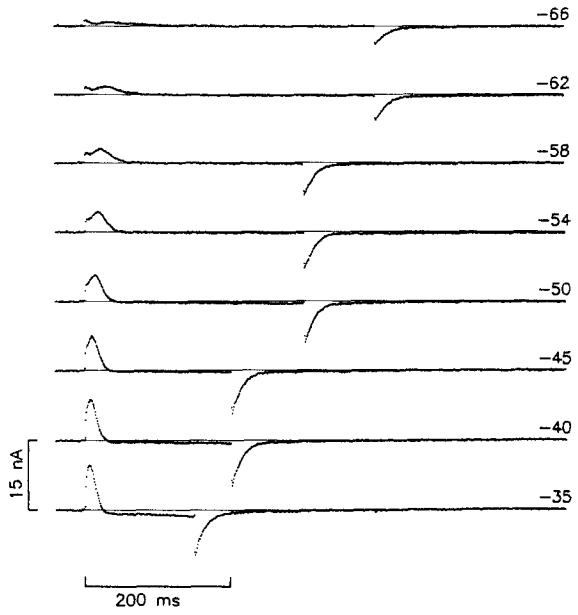

FIGURE 1. TEST minus CONTROL currents in a cut fiber bathed in a methane sulfonate solution. Fiber identification: 80112. Diameter, 112 μm. Saponin treatment was applied to membrane segments in both end pools at time zero. After rinsing, the solutions in the end pools were replaced by solution B. Then the solution in the center pool was changed to a TEA.$MeSO_3$ solution (solution F). At the 20th minute, the voltage clamp was turned on and the holding potential was set at −90 mV. Traces were taken from the 57th to the 77th minute, during which the holding current changed from −39 to −52 nA and $r_e/(r_e + r_i)$ decreased from 0.984 to 0.977. The numbers at the right show the potentials during the TEST pulses. Only representative traces are shown.

In the experiment shown in Fig. 2, charge movements in the TEA.Cl and TEA.$MeSO_3$ solutions were compared. TEST minus CONTROL current traces were recorded in the TEA.Cl solution first (Fig. 2 *A*). Prominent I_γ humps can be seen clearly in the ON segments of the second to the fourth traces. When the TEA.Cl solution was replaced by the TEA.$MeSO_3$ solution, the positive pedestals due to maintained ionic current in the ON segments were replaced by negatively sloping baselines up to about −40 mV (Fig. 2 *B*). Beyond that potential, the ON segments showed a sloping baseline plus a negative pedestal. In addition to the change in maintained current, the shape of I_γ was altered, with the largest difference detectable at −46 mV. This change in shape could be due to a voltage shift in the kinetics of I_γ, as will be explained below. These effects of $MeSO_3^-$ were partially reversed when the

center pool solution was changed back to the TEA.Cl solution, as revealed by traces in Fig. 2 *C*. The negative pedestals in the ON segments disappeared, but not the negatively sloping baselines. I_γ humps can be seen in the first four traces, but the shapes of the humps were still different from those in the corresponding traces in Fig. 2 *A*.

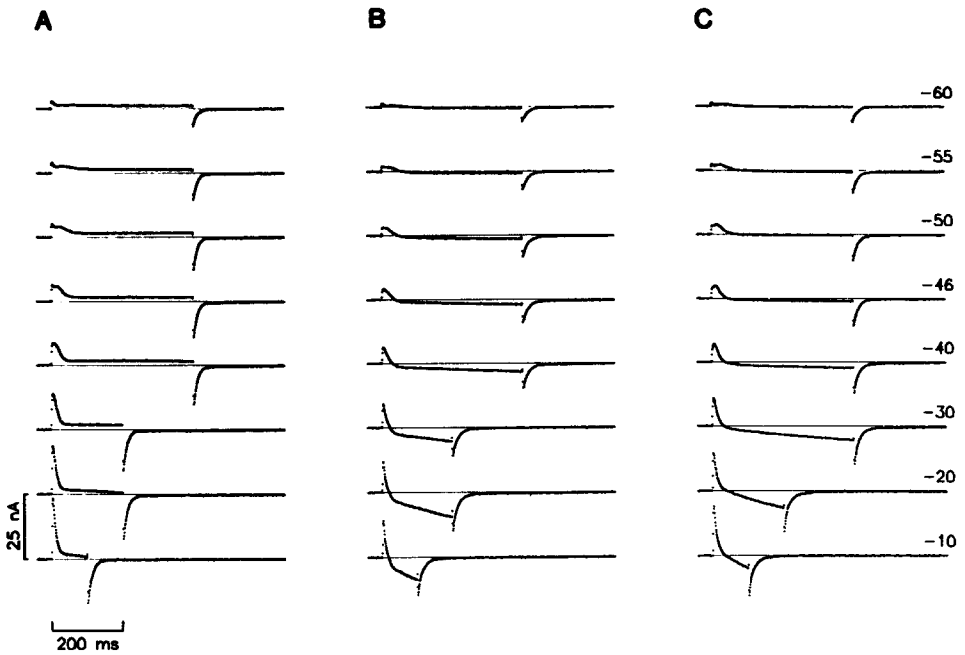

FIGURE 2. Effect of substituting Cl^- by $MeSO_3^-$ on TEST minus CONTROL currents in a cut fiber. Fiber identification: 85231. Diameter, 118 μm. Saponin treatment was applied to membrane segments in both end pools at time zero. After rinsing, the solutions in the end pools were replaced by solution B. Then, the solution in the center pool was changed to a TEA.Cl solution (solution D). At the 22nd minute, the voltage clamp was turned on and the holding potential was set at −90 mV. From the beginning to the end of the experiment, the holding current changed from −46 to −50 nA and $r_e/(r_e + r_i)$ remained constant at 0.980. (*A*) Traces taken in solution D from the 57th to the 74th minute. At the 138th minute, the center pool solution was changed to solution F. (*B*) Traces taken from the 145th to the 162nd minute. At the 166th minute, the center pool solution was changed back to solution D. (*C*) Traces taken from the 175th to the 194th minute. Only representative traces are shown in each panel. The numbers at the right show the potentials during the TEST pulses (same pulse for the traces in each row).

The amounts of ON and OFF charge were estimated (see Hui and Chandler, 1990) by integrating the areas of the ON and OFF transients in the traces of Fig. 2 (and others not shown), and are plotted against the TEST pulse potential in Fig. 3 as diamonds (for control TEA.Cl solution), squares (for TEA.$MeSO_3$ solution), and triangles (for washout TEA.Cl solution). Filled symbols represent OFF charge and

open symbols ON charge. ON charge that overlaps with the corresponding OFF charge is not shown. Also, ON charge at the potentials at which the I_γ hump was broad (around −60 to −55 mV) was not estimated because baseline fit was unreliable (see Hui and Chandler, 1990; Hui, 1991).

Several observations can be made before detailed data analysis. In the TEA.Cl solution, ON and OFF charges were equal within experimental error, except at 0 mV. When Cl^- was replaced by $MeSO_3^-$, ON:OFF charge equality was preserved up to −40 mV, beyond which the amount of OFF charge exceeded the corresponding amount of ON charge, probably due to contamination of inward ionic current. The steep portion of the *Q-V* plot is shifted slightly to the left; the maximum amount of total charge is reduced; and the shoulder where the slope of the *Q-V* plot turned from the steep portion to the less steep portion is lowered, implying that the maximum

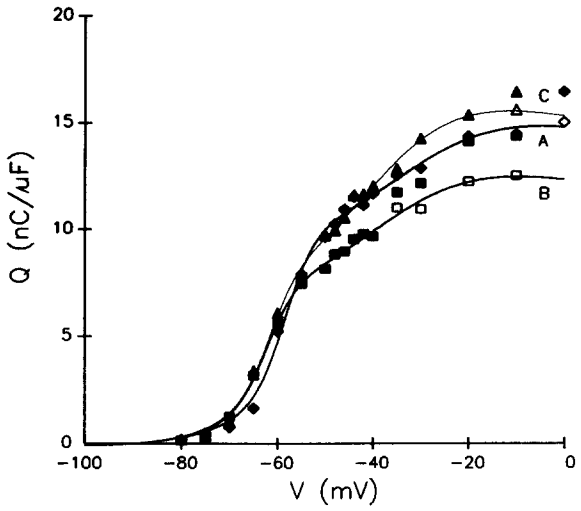

FIGURE 3. Steady-state voltage distributions of total charge in a cut fiber bathed in a TEA.Cl or TEA.$MeSO_3$ solution. Same fiber as in Fig. 2. Diamonds show data taken with TEA.Cl (control), squares with TEA.$MeSO_3$, and triangles with TEA.Cl (bracketing), in the center pool solution. Open symbols represent ON charge and filled symbols represent OFF charge. The points were obtained from the time integrals of ON or OFF transients in TEST minus CONTROL current traces, some of which are shown in Fig. 2. The smooth curves A–C were obtained by least-squares fits of a sum of two Boltzmann distribution functions to the three data sets. In each data set, ON charge was used for the fit when both ON and OFF charges are shown at the same potential; otherwise, OFF charge was used. The values of the best-fit parameters are listed in the first three rows of Table II.

amount of Q_γ was reduced. When the center pool solution was changed back to the TEA.Cl solution, the reduction in total charge was reversed. In fact, the amounts of charge above −40 mV in curve C are slightly larger than the corresponding amounts in curve A. However, the voltage shift of the steep portion of the plot is not reversed and the shoulder is less marked. Even in the presence of negatively sloping baselines in the ON segments of the traces in Fig. 2 *C*, ON:OFF charge equality was still preserved up to −20 mV and the amounts of OFF charge in these traces were similar to the corresponding amounts in the traces of Fig. 2 *A*. This suggests that there is no correlation between the negatively sloping baseline in the ON segment and the ionic contamination on OFF charge at large depolarizations.

To assure that the maintained, apparently inward ionic current does not generate a tail current to contaminate the OFF charge, charge movement was studied in another

fiber, bathed in the TEA.$MeSO_3$ solution, with TEST pulses of varying durations. The negative pedestal began to appear in the ON segments of TEST minus CONTROL current traces at −50 mV. With larger depolarizations, the magnitude of the pedestal was increased and the negative slope of the baseline became more steep, the same as the traces in Fig. 2 *B*. Three TEST pulses to −45 mV, of durations 200, 300, and 400 ms, were applied in the early phase of the experiment, and the amounts of OFF charge were 8.4, 8.8, and 8.6 nC/μF, respectively, which were almost identical to the amount of ON charge, 8.5 nC/μF, within experimental error. Two other sequences of TEST pulses to −45 mV were applied halfway through and at the end of the experiment by including the durations of 100 and 600 ms. The amounts of OFF charge in all the runs were 8–9 nC/μF, indicating that the fiber was absolutely stable. At −40 and −35 mV, OFF charge was still invariant for pulse durations of 100–300 ms and had values of 9.8–10.4 and 11.1–12.5 nC/μF, respectively.

The TEST current trace from a run at −40 mV and the associated CONTROL current trace were examined at high gain. The ON segment of the CONTROL current trace was absolutely flat and the negative slope of the ON baseline in the TEST minus CONTROL current trace was originated in the TEST current. In addition, although the TEST pulse was 2.5 times as large as the CONTROL pulse, the magnitude of the ionic current at the beginning of the TEST pulse was only 2.35 times the maintained ionic current during the CONTROL pulse. Thus, when the CONTROL current was scaled up 2.5 times and subtracted from the TEST current, the slight mismatch in the ionic current yielded the negative pedestal. This rectifying property is characteristic of $MeSO_3^-$, as it does not occur when Cl^- is used. The negative slope mentioned above must then be due to a time-dependent change in the flux of $MeSO_3^-$. On repolarization, the change should reverse in direction. However, the invariance in OFF charge with increasing pulse durations implied that the change in flux on repolarization probably lasted hundreds of milliseconds, or even longer, and so was buried in the OFF baseline.

The situation was different with more depolarized TEST pulses. At −30 mV, the amounts of OFF charge were 13.3, 14.8, and 18.9 nC/μF for pulse durations of 150, 200, and 300 ms, while the ON charge was 13.6 nC/μF. At −20 mV, the amounts of OFF charge were 17.9, 22.9, and 29.2 nC/μF for pulse durations of 100, 150, and 200 ms, while the ON charge was 17.5 nC/μF. Thus, at these potentials another inward ionic current, distinct from the current described above, was activated and its tail current contaminated the OFF charge progressively more with increasing pulse durations. This latter current is probably related to the slow Ca current and is generally noticeable as it has a waveform similar to those shown in the ON segments of the last two traces in Fig. 7 *A*. It should be noted that, in this fiber, if the durations of the TEST pulses at −30 and −20 mV were not longer than 150 and 100 ms, respectively, the contamination of OFF charge by the tail Ca current was not substantial.

The smooth curves A–C in Fig. 3 were obtained by fitting a sum of two Boltzmann distribution functions to the three data sets. In each data set, any open symbol shown was used to replace the corresponding filled symbol in the fit. The best-fit parameters of the three curves are listed in Table II as the first entry. The features described above were confirmed by the values of the parameters; namely, $\overline{V}_\gamma$ in curve B was 4–5

mV more negative than that in curve A. The value of q_{max}/c_m for either Q_γ or the total charge (Q_β + Q_γ) in curve B was 2–3 nC/μF smaller than the corresponding value in curve A. After washout, the value of $\overline{V}_\gamma$ in curve C was not restored to the control value but stayed close to the value in curve B. The values of q_{max}/c_m for the total charge were similar in curves A and C. The smaller amount of total charge above −40 mV in curve A than in curve C can be explained by the larger value of k_β in curve A, such that the curve did not reach saturation at 0 mV but would rise to the same asymptotic value as curve C. The disappearance of the shoulder in curve C can also be explained by a smoother transition from the steeper portion to the less steep portion.

TABLE II

Effect of Replacing Cl^- in the Bathing Solution by $MeSO_3^-$ on Q-V Distributions of Q_β and Q_γ in Cut Fibers

(1) Fiber reference	(2) External solution	(3) c_m	(4) $\overline{V}_\beta$	(5) k_β	(6) $q_{\beta,max}/c_m$	(7) $\overline{V}_\gamma$	(8) k_γ	(9) $q_{\gamma,max}/c_m$	(10) (9)/((6)+(9))
		μF/cm	mV	mV	nC/μF	mV	mV	nC/μF	%
85231	Cl^-	0.193	−34.2	10.7	8.6	−60.4	3.3	11.1	56.4
	$MeSO_3^-$	0.192	−40.1	10.8	9.0	−65.1	3.3	8.3	47.9
	Cl^-	0.181	−41.1	9.4	11.9	−64.0	3.3	8.6	42.0
85241	Cl^-	0.194	−38.8	9.6	8.3	−56.6	2.1	13.9	62.6
	$MeSO_3^-$	0.193	−42.7	9.1	12.5	−63.8	2.5	11.1	47.0
85311	Cl^-	0.145	−27.7	12.3	11.3	−58.6	3.9	18.3	61.8
	$MeSO_3^-$	0.150	−26.9	12.6	10.1	−62.3	2.9	15.3	60.2
	Cl^-	0.139	−37.7	11.0	11.7	−63.4	2.5	14.9	56.0
86241	Cl^-	0.099	−40.3	6.8	10.9	−57.3	1.4	12.8	54.0
	$MeSO_3^-$	0.097	−37.4	9.9	11.3	−62.2	4.0	13.1	53.7
	Cl^-	0.091	−48.1	6.5	12.0	−63.0	2.6	11.4	48.7

Column 1 gives fiber identifications. Columns 2 and 3 give the major anions in the center pool solution and the values of c_m, respectively. Columns 4–9 give the best-fit values of the parameters in the Boltzmann distribution functions of Q_β and Q_γ, with CONTROL charge correction and gap correction. Column 10 gives the fractions of Q_γ in the total charge.

The left shift of $\overline{V}_\gamma$ when Cl^- was replaced by $MeSO_3^-$ can explain, to some extent, the apparent change in the kinetics of I_γ in the ON segments of the traces in Fig. 2 *B*. To allow for the voltage shift, the first trace in Fig. 2 *B* should be compared with the second trace in Fig. 2 *A*, and so forth. Indeed, after the shift, the kinetics of I_γ in the two solutions was comparable. After washout, the shift in $\overline{V}_\gamma$ was not reversed. This can also explain why the humps in the ON segments of the traces in Fig. 2 *C* resembled the corresponding ones in Fig. 2 *B* more than those in Fig. 2 *A*.

Three other similar experiments were performed and the results are summarized in Table II. In all the fibers, $MeSO_3^-$ shifted the value of $\overline{V}_\gamma$ by 4–7 mV in the hyperpolarizing direction and the effect was not reversed after washout. The slight suppression of Q_γ in Fig. 3 by $MeSO_3^-$ was shared by two of the three other fibers.

In seven other experiments, including the one shown in Fig. 1, the fibers were not exposed to Cl^- and charge movement was measured in the $TEA.MeSO_3$ solution only. The *Q-V* plots were fitted by a sum of two Boltzmann distribution functions. The mean values of the parameters for Q_β and Q_γ from these seven fibers and the four fibers in Table II are listed in Table III. For comparison, the mean values in the TEA.Cl solution from Hui (1991) and those in the TEA_2SO_4 solution from Hui and Chandler (1990) are also listed.

The values in the $TEA.MeSO_3$ solution are quite close to those in the TEA.Cl solution. $\overline{V}_\beta$ appears to be more negative, and $q_{\beta,max}/c_m$ and $q_{\gamma,max}/c_m$ appear to be smaller, in the $TEA.MeSO_3$ solution than in the TEA.Cl solution, but the differences are statistically insignificant ($P > 0.05$ with the two-tailed *t* test). The fraction of Q_γ in the total charge is almost identical in the two solutions ($P > 0.5$ with the two-tailed *t*

TABLE III

Comparison of Q-V Distributions of Q_β and Q_γ in Cut Fibers Bathed in Solutions with Different Major Anions

(1) External solution	(2) No. of fibers	(3) Gap factor	(4) $\overline{V}_\beta$	(5) k_β	(6) $q_{\beta,max}/c_m$	(7) $\overline{V}_\gamma$	(8) k_γ	(9) $q_{\gamma,max}/c_m$	(10) (9)/((6)+(9))
			mV	*mV*	*nC/μF*	*mV*	*mV*	*nC/μF*	%
Cl^-	29	0.986	−33.0	10.9	11.2	−56.1	2.9	12.0	51.3
		±0.001	±1.3	±0.4	±0.5	±0.6	±0.2	±0.7	±1.7
$MeSO_3^-$	11	0.983	−37.1	11.7	9.7	−62.5	3.1	10.0	50.1
		±0.002	±1.5	±0.5	±0.6	±0.8	±0.2	±0.9	±2.6
SO_4^{2-}	5	0.978	−20.0	17.0	36.4	−41.6	2.5	11.8	24.2
		±0.004	±3.3	±2.0	±2.3	±1.4	±0.8	±1.7	±2.2

Columns 1 and 2 give the major anions in the center pool solution and the number of fibers studied in the groups. Column 3 gives the average values of $r_e/(r_e + r_i)$. Columns 4–9 give the average best-fit values of the parameters in the Boltzmann distribution functions of Q_β and Q_γ, with CONTROL charge correction and gap correction. Column 10 gives the average fractions of Q_γ in the total charge for the fibers in each group. Results of Cl experiments are from Table VI of Hui (1991). Results of SO_4 experiments are from Table VI of Hui and Chandler (1990).

test). The only significant difference is in $\overline{V}_\gamma$, which is 6 mV more negative in the $TEA.MeSO_3$ solution than in the TEA.Cl solution ($P < 0.001$ with the two-tailed *t* test). Although the shift in $\overline{V}_\beta$ is insignificant, it is parallel to the shift in $\overline{V}_\gamma$. In contrast, the voltage distributions of Q_β and Q_γ are affected to a larger extent by SO_4^{2-}: k_γ and $q_{\gamma,max}/c_m$ are not changed ($P > 0.5$ with the two-tailed *t* test); $\overline{V}_\beta$ and $\overline{V}_\gamma$ are 13–15 mV less negative in the TEA_2SO_4 solution than in the TEA.Cl solution; k_β is increased by ~50% in the TEA_2SO_4 solution; and $q_{\beta,max}/c_m$ is increased more than twofold in the TEA_2SO_4 solution, making the fraction of Q_γ in the total charge decrease from one-half to one-fourth. The latter differences are highly significant ($P < 0.001$ with the two-tailed *t* test).

Results in this section show that, although the shape of I_γ was affected by replacing Cl^- with $MeSO_3^-$, probably due to a negative shift in $\overline{V}_\gamma$, prominent I_γ humps could

still be observed in the TEA.$MeSO_3$ solution. $MeSO_3^-$ also suppressed the amount of Q_β or Q_γ in some fibers, but on the average the suppression is statistically insignificant.

Effect of Removal of Intracellular Creatine Phosphate on Charge Movement

Cut skeletal muscle fibers have many advantages over intact fibers for studying charge movement and other signals involved in excitation–contraction coupling. Unfortunately, these advantages are undermined by at least one complication: since the plasma membranes of the end pool segments of a cut fiber are either notched or permeabilized, myoplasmic constituents that may be vital in maintaining the physiological state of the fiber can diffuse out of the fiber. This problem can be avoided by making the end pool solution as close in composition to the myoplasm as possible. Since creatine phosphate is normally present in the myoplasm at a concentration as high as 50 mM (Godt and Maughan, 1988), we generally included 20 mM creatine phosphate in the end pool solution (Hui and Chandler, 1990; Hui, 1991), but other workers who measured charge movement in cut fibers did not. Thus, experiments were performed to compare the properties of charge movement in the presence and absence of 20 mM creatine phosphate in the end pool solution.

Fig. 4 *A* shows TEST minus CONTROL current traces elicited in a cut fiber by a 400-ms TEST pulse to −40 mV. Trace 1 was recorded with 20 mM creatine phosphate in the end pool solution (solution B in Table I). The ON segment shows an early I_β component and an I_γ component manifested as a hump in the decay phase of I_β, same as in other cut or intact fibers. After trace 1 was taken, creatine phosphate was removed from the end pool solution (solution C in Table I). Five runs were taken, of which three are shown as traces 2–4. In these traces, the amplitude of the hump became progressively smaller, and 25 min after the removal of creatine phosphate no I_γ could be resolved in trace 4. In other control experiments in which creatine phosphate was not removed, the I_γ hump generally remained unchanged for several hours. After trace 4 was taken, 20 mM creatine phosphate was restored in the end pool solution and many TEST minus CONTROL current traces (not shown) were taken. In trace 5, which was taken 62 min after the restoration of creatine phosphate, an I_γ hump can be visualized in the ON segment; however, it is not as prominent as that in trace 1, suggesting that the diminution of the I_γ hump with creatine phosphate removal was partially reversible.

The amount of OFF charge in each trace of Fig. 4 *A* (and other traces not shown), estimated by integrating the area of the OFF current transient, is plotted as a function of time in the upper panel of Fig. 4 *C*. The concentration of creatine phosphate in the end pool solution is shown by the solid line in the lower panel. 20 mM creatine phosphate was present in the end pool solution from the beginning of the experiment. After equilibration for ~1 h, the concentration of creatine phosphate in the myoplasm in the center pool region was assumed to be 20 mM. When creatine phosphate was removed from the end pool solution, creatine phosphate in the myoplasm presumably diffused into the end pools, lowering its concentration in the center pool region. The approximate average concentration in the center pool region was estimated by Eq. 2.15 in Crank (1956), assuming a diffusion constant of 2×10^{-6} cm^2/s. The average concentration is plotted as the decaying portion of the

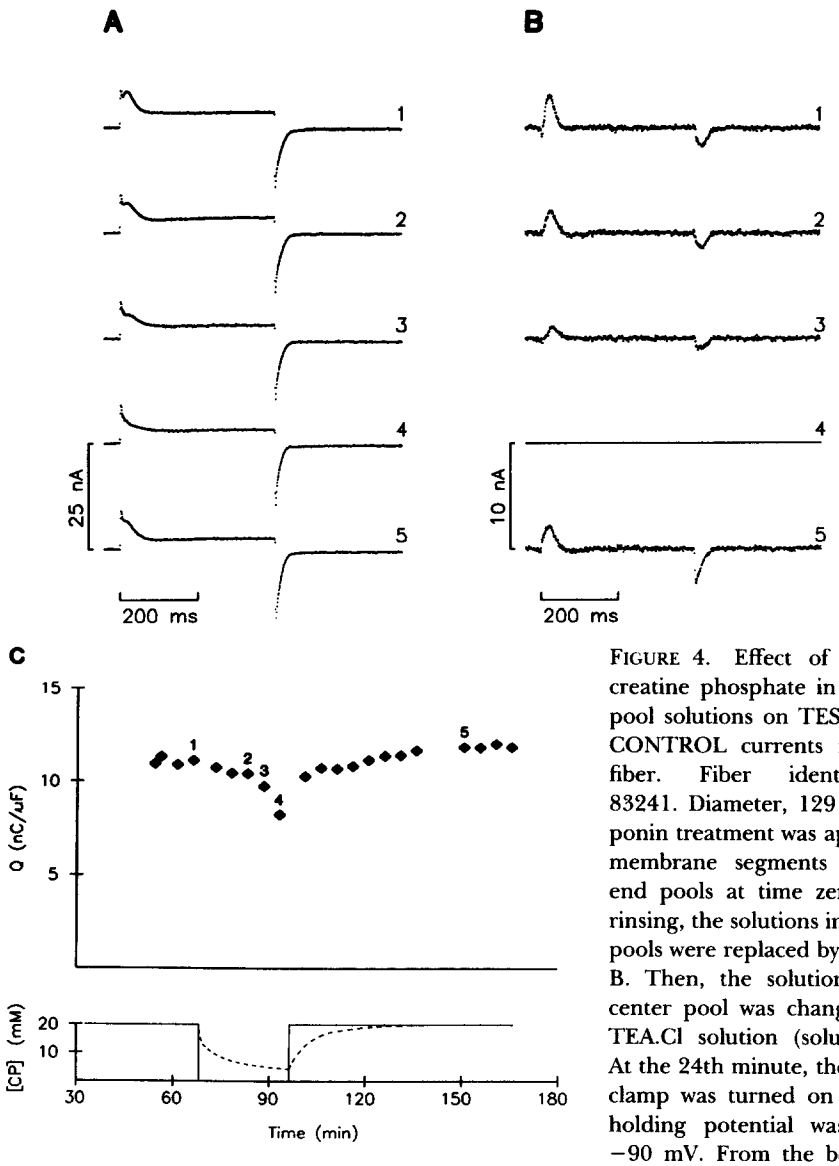

FIGURE 4. Effect of 20 mM creatine phosphate in the end pool solutions on TEST minus CONTROL currents in a cut fiber. Fiber identification: 83241. Diameter, 129 μm. Saponin treatment was applied to membrane segments in both end pools at time zero. After rinsing, the solutions in the end pools were replaced by solution B. Then, the solution in the center pool was changed to a TEA.Cl solution (solution D). At the 24th minute, the voltage clamp was turned on and the holding potential was set at −90 mV. From the beginning to the end of the experiment, the holding current changed from −45 to −58 nA and $r_e/(r_e + r_i)$ decreased from 0.988 to 0.983. (*A*) TEST minus CONTROL traces elicited by a TEST pulse to −40 mV. The times at which the traces were taken and the end pool solutions were changed can be obtained from *C*. (*B*) Difference traces from *A* obtained by subtracting trace 4 from each trace. (*C*) The upper panel shows the amounts of OFF charge estimated from the traces in *A* (numbered correspondingly) and other traces not shown. The lower panel shows the concentration of creatine phosphate in the end pool solution.

dashed curve in the lower panel. When 20 mM creatine phosphate was restored in the end pool solution, it diffused back into the myoplasm, increasing its concentration in the center pool region. The approximate average concentration in the center pool region was estimated by Eq. 4.17 in Crank (1956) and is plotted as the rising portion of the dashed curve.

The upper panel shows that, after the removal of creatine phosphate, there was a progressive decrease in OFF charge parallel to the slow disappearance of I_γ in the ON segment, implying that there was an actual loss of Q_γ. When 20 mM creatine phosphate was restored, the amount of OFF charge recovered fully, whereas the shape of I_γ in the ON segment did not (compare traces 1 and 5 in Fig. 4 *A*).

If creatine phosphate removal has no effect on the ON time course of I_β at −40 mV, then the waveform of the I_γ hump in traces 1–3 and 5 of Fig. 4 *A* can be obtained by subtracting trace 4 from each trace. The first three difference traces in Fig. 4 *B* show that the I_γ humps in the ON segments are bell shaped, as was suggested for I_γ in

TABLE IV

Effect of Removing Creatine Phosphate on I_γ

(1) Trace No.	(2) [CP]	(3) c_m	(4) ON transient $\Delta t_{1/2}$	(5) ON transient t_p	(6) ON transient Area	(7) OFF transient $\Delta t_{1/2}$	(8) OFF transient t_p	(9) OFF transient Area
	mM	*μF/cm*	*ms*	*ms*	*nC/μF*	*ms*	*ms*	*nC/μF*
1	20	0.259	25.2	22.8	3.05	32.4	20.5	2.88
2	0	0.260	27.7	25.1	2.38	31.4	21.1	2.18
3	0	0.258	25.4	29.4	1.56	27.2	19.2	1.51
4	0	0.256	—	—	0	—	—	0
5	20	0.250	33.1	22.2	3.37	17.7	4.3	3.63

Same fiber as in Fig. 4. Columns 1 and 2 give the trace numbers in Fig. 4 *B* and the concentrations of creatine phosphate in the end pool solution when the trace was taken. Column 3 gives the values of c_m. Columns 4–6 give the half-widths, the times-to-peak, and the amounts of charge in the ON transients of the traces. Columns 7–9 give the corresponding information for the OFF transients.

intact fibers (Hui, 1983*b*). The first three points in the ON segment of trace 1 are below the baseline, implying that there might be some minor change in the magnitude or kinetics of I_β at this potential after the removal of creatine phosphate. The OFF transients of the traces show a marked rising phase, which has not been observed in intact or cut fibers. The half-widths, times-to-peak, and areas of the ON and OFF transients of the traces in Fig. 4 *B* are listed in Table IV. The numbers in columns 5 and 8 show that the amounts of ON and OFF charge in each trace were almost equal, within experimental error. It will be shown in the following experiment (Figs. 5 and 6) that this equality might not be held at more negative potentials. The amount of charge in trace 1 of Fig. 4 *B* provided a lower limit to the amount of Q_γ in trace 1 of Fig. 4 *A*, but the actual amount of Q_γ could be larger if trace 4 of Fig. 4 *A* contained some residual Q_γ or an increased amount of Q_β.

Table IV also shows that, after the removal of creatine phosphate, the amount of ON or OFF charge diminished progressively and the time-to-peak of the ON

transient was somewhat prolonged. When creatine phosphate was restored, the amount of Q_γ recovered completely but the time course of I_γ did not. The change in the shape of I_γ from trace 1 to trace 5 could be due to a chronic effect of creatine phosphate removal. Four other experiments showed similar reversible disappearance of I_γ in the ON segment and reversible reduction in the amount of OFF charge due to creatine phosphate removal.

The experiment in Fig. 4 was performed with a constant TEST pulse to −40 mV, which is usually at the upper edge of the steep portion of a Q-V curve. If creatine phosphate removal causes the Q_γ-V curve to be shifted in the depolarizing direction such that the lower edge of the steep portion is at −40 mV after the shift, that would result in the apparent reduction of Q_γ. The experiment in Figs. 5 and 6 was carried out to rule out this possibility by comparing the steady-state voltage distribution of charge in the presence and absence of 20 mM creatine phosphate.

With creatine phosphate in the end pool solution, a distinct I_γ hump can be visualized in the ON segments of the traces (thick traces in Fig. 5 *A*) recorded at TEST pulse potentials between −60 and −40 mV. At ≥ −30 mV, it is difficult to resolve I_γ from I_β. After the removal of creatine phosphate from the end pool solution, no humps can be visualized in the ON segments (thin traces in Fig. 5 *A*) over a wide range of potential, indicating that the disappearance of the I_γ hump was not due to a shift in the voltage dependence of the kinetics of I_γ. In addition, the OFF currents in the thin traces decay faster than those in the thick traces. This difference in OFF kinetics could be due to a direct effect of creatine phosphate on the kinetics of OFF current. Alternatively, if I_γ has slower OFF kinetics than I_β (Hui and Chandler, 1991), that would make the OFF currents in the thick traces decay slower than those in the thin traces. A similar difference in the rate of decay of OFF current also existed between traces 1 and 4 of Fig. 4 *A*, but was less marked, probably because that fiber had less I_γ.

In Fig. 6 *A*, the amounts of ON charge (open symbols) and OFF charge (filled symbols) from the traces in Fig. 5 (and others not shown) are plotted against the potentials during the TEST pulses. The diamonds represent the amounts of charge in the presence of creatine phosphate. Between −55 and −45 mV, ON charge is smaller than OFF charge. The difference is caused by the broad waveforms of the I_γ humps at these potentials, resulting in unreliable fittings of the ON baselines (Hui and Chandler, 1990). Thus, from −80 to −30 mV, OFF charge is taken to represent the total charge. At −20 and −10 mV, OFF charge is larger than ON charge, probably because of contamination by tail Ca current (Hui and Chandler, 1990). ON charge is therefore taken to represent the total charge at these two potentials. Curve 1 was fitted to the mentioned filled and open diamonds by a sum of two Boltzmann distribution functions. The values of $\overline{V}_\beta$, k_β, $q_{\beta,max}/c_m$, $\overline{V}_\gamma$, k_γ, and $q_{\gamma,max}/c_m$ are −38.2 mV, 8.2 mV, 10.5 nC/μF, −58.2 mV, 2.4 mV, and 8.9 nC/μF, respectively. Thus, in the presence of creatine phosphate, Q_β and Q_γ existed in this fiber in approximately equal amounts, in agreement with the results in preceding papers (Hui and Chandler, 1990; Hui, 1991).

After the removal of creatine phosphate, the amount of ON or OFF charge at each potential (squares) was reduced. Between −60 and −40 mV, ON charge is smaller than OFF charge, similar to the situation with creatine phosphate, but the removal of

creatine phosphate appears to enhance the discrepancy between ON and OFF charges, suggesting that, without creatine phosphate, more I_γ is buried in the baseline of the ON segment, particularly around −50 mV. Indeed, in the thin trace of the fourth pair in Fig. 5 *A*, although the ON transient only shows a fast I_β component, it is impossible to rule out the presence of an I_γ hump having an extremely broad time course and an unresolvable amplitude. Only with the presence of this obscured

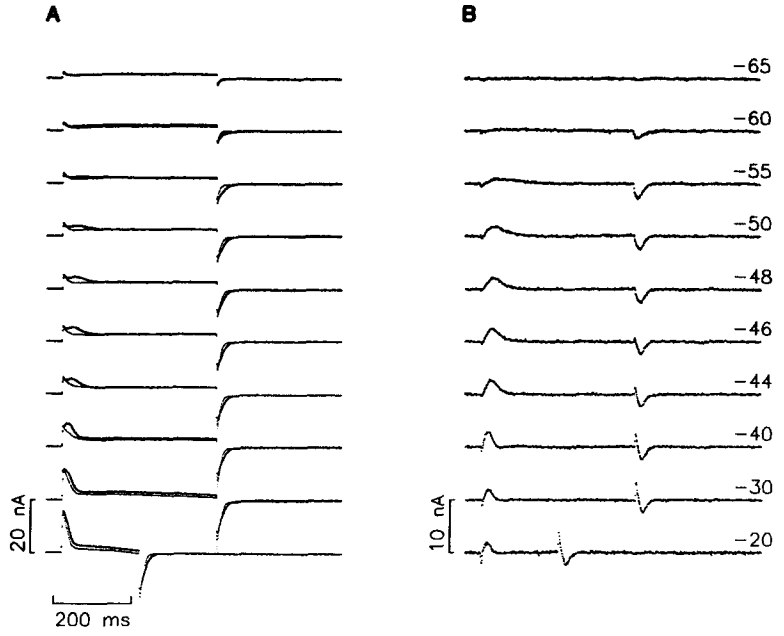

FIGURE 5. TEST minus CONTROL currents in a cut fiber with and without 20 mM creatine phosphate in the end pool solution. Fiber identification: 83231. Diameter, 121 μm. Saponin treatment was applied to membrane segments in both end pools at time zero. After rinsing, the solutions in the end pools were replaced by solution B. Then the solution in the center pool was changed to a TEA.Cl solution (solution D). At the 21st minute, the voltage clamp was turned on and the holding potential was set at −90 mV. The holding current and $r_e/(r_e + r_i)$ remained constant at −29 nA and 0.991, respectively, throughout the experiment. (*A*) Thick traces were taken with 20 mM creatine phosphate (solution B) in the end pools from the 58th to the 86th minute. At the 90th minute, the end pool solutions were replaced by a creatine phosphate–free solution (solution C). Thin traces were taken from the 113th to the 130th minute. (*B*) Difference traces obtained by subtracting each thin trace in *A* from the superimposed thick trace. The numbers at the right show the potentials during the TEST pulses (same pulse for the traces in *A* and *B*). Only representative traces are shown in each panel.

I_γ would the ON:OFF charge equality be preserved. At −20 and −10 mV, OFF charge (filled squares) in Fig. 6 *A* is larger than ON charge (open squares), the same as with creatine phosphate. Thus, the filled squares up to −30 mV and the open squares at −20 and −10 mV are taken to represent the total charge in the absence of creatine phosphate.

A comparison of the two sets of data in Fig. 6 *A* show that the steep rise of the filled

diamonds between −65 and −55 mV and the shoulder at around −55 mV disappear in the filled squares. An attempt was made to fit a sum of two Boltzmann distribution functions to the squares, but the fitting routine did not converge. The points were therefore fitted by a single Boltzmann distribution function, as shown by curve 2. The best-fit values for $\bar{V}$, k, and q_{max}/c_m were −45.2 mV, 6.5 mV, and 15.4 nC/μF, respectively. The value of q_{max}/c_m in curve 2 is 4 nC/μF smaller than the sum of $q_{\beta,max}/c_m$ and $q_{\gamma,max}/c_m$ in curve 1, implying that the total amount of charge was reduced after the removal of creatine phosphate. It should be noted that this difference is larger

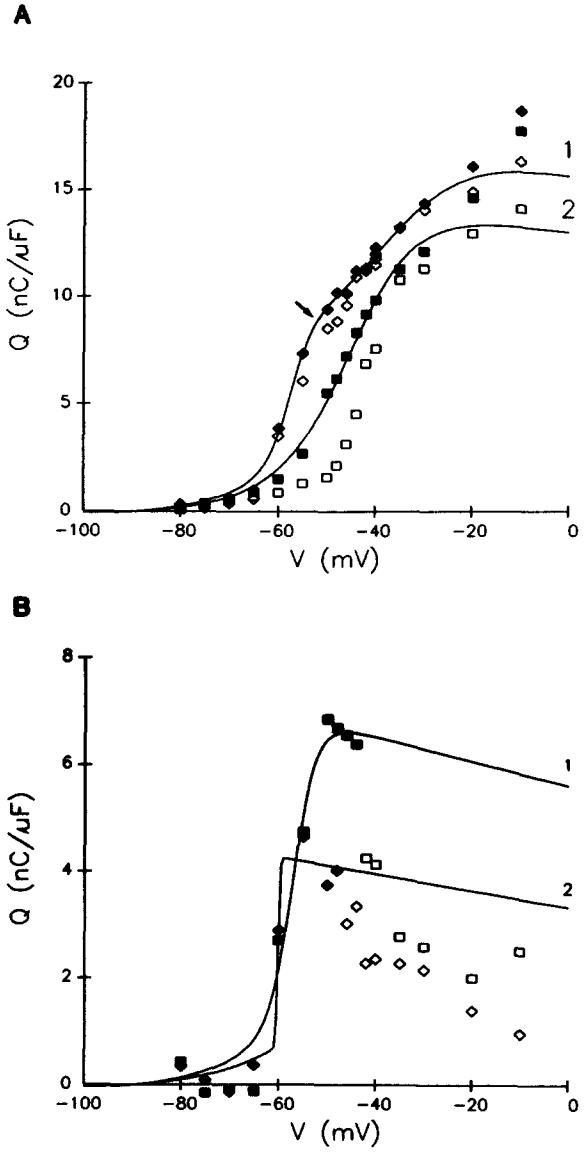

FIGURE 6. Steady-state voltage distributions of total charge in a cut fiber with and without 20 mM creatine phosphate in the end pool solutions. Same fiber as in Fig. 5. (*A*) Diamonds show data taken with, and squares without, 20 mM creatine phosphate in the end pool solutions. Open symbols represent ON charge and filled symbols represent OFF charge. The points were obtained from the time integrals of either ON or OFF transients in TEST minus CONTROL current traces, some of which are shown in Fig. 5, *A* and *B*. Curves 1 and 2 were obtained by least-squares fits of a sum of two Boltzmann distribution functions and of a single Boltzmann distribution function, respectively. In each data set, the values of ON charge at −20 and −10 mV were used for the fit; at other potentials, the values of OFF charge were used. (*B*) Squares were obtained from the time integrals of ON transients and diamonds from OFF transients in the difference current traces, some of which are shown in Fig. 5 *B*. The smooth curves were obtained by least-squares fits of a single Boltzmann distribution function to the two data sets, with open symbols excluded from the fit.

than the difference between the open diamond and the open square at −10 mV, which is ~2 nC/μF. This apparent discrepancy arises as a result of gap correction and CONTROL charge correction, as explained in the Methods section of the preceding paper (Hui, 1991).

The 4 nC/μF decrease in total charge was too small to account for all the Q_γ in curve 1, which amounted to 8.9 nC/μF. To understand the reason for the difference, each thin trace in Fig. 5 *A* was subtracted from the thick trace at the same potential. In the difference traces shown in Fig. 5 *B*, the ON transients are bell shaped and the OFF transients have a pronounced rising phase, similar to the traces in Fig. 4 *B*. For potentials > −48 mV, the OFF transients show a positive deflection preceding the usual negative deflection. This biphasic nature is also present in the ON transients, but to a smaller extent. The positive (negative) deflections in the OFF (ON) transients could be due to an increase in the peak amplitude of I_β when creatine phosphate was removed.

The amount of charge in each trace of Fig. 5 *B* is plotted as a function of potential in Fig. 6 *B*. The squares, representing ON charge, were obtained by subtracting the open squares in Fig. 6 *A* from the corresponding open diamonds. Likewise, the diamonds in Fig. 6 *B*, representing OFF charge, were obtained by subtracting the filled squares in Fig. 6 *A* from the corresponding filled diamonds. For potentials < −50 mV, ON charge and OFF charge are roughly equal. The points rise sharply at −60 mV. OFF charge begins to decline at −50 mV, while ON charge continues to increase before declining. The largest difference between ON and OFF charges is at around −50 mV, as explained above.

Because of all the complications, the difference *Q-V* plots of both ON and OFF charges were studied. Each plot was fitted by a single Boltzmann distribution function. The points represented by the open symbols were excluded from the fits because they correspond to the ON or OFF transients that are biphasic. For the ON charge (curve 1) the values of $\bar{V}$, k, and q_{max}/c_m are −57.8 mV, 2.4 mV, and 8.0 nC/μF, respectively, whereas for the OFF charge (curve 2) the values are −61.0 mV, 0.2 mV, and 5.1 nC/μF, respectively. The value of k in curve 2 is exceptionally small and the value of q_{max}/c_m is smaller than the value of $q_{\gamma,max}/c_m$ of the Q_γ component in curve 1 of Fig. 6 *A*. On the other hand, the values of the parameters in curve 1 of Fig. 6 *B* are very close to the values of the Q_γ component in curve 1 of Fig. 6 *A*, but some of the points used for the fit lie in the potential range in which the fitting of baseline is uncertain. Thus, there is some uncertainty about the exact amount of charge suppressed as a result of creatine phosphate removal. Nonetheless, there is no doubt that at least 4 nC/μF of charge was suppressed when creatine phosphate was removed. The exact amount suppressed is likely to be less than the 8.9 nC/μF of Q_γ in the presence of 20 mM creatine phosphate, because creatine phosphate in the myoplasm had not completely diffused out (see dashed curve in the lower panel of Fig. 4 *C*). Moreover, there could be an increase in Q_β when creatine phosphate was removed, as hinted by the biphasic nature of the current transients at large depolarizations. Whether the increase in Q_β is due to an interconversion from Q_γ remains to be clarified (see Discussion), but the increase in Q_β, if it occurred, was definitely smaller than the decrease in Q_γ.

Two other experiments were performed with the order of solution change reversed. Since the fibers were equilibrated in creatine phosphate–free end pool

solution from the beginning of the experiment, the residual concentration of creatine phosphate in the myoplasm of the center pool region should be negligible. TEST minus CONTROL current traces from both fibers did not show any I_γ hump in the ON segments. When the Q-V plots were fitted by a sum of two Boltzmann distribution functions, the fitting routine did not converge. When the plots were fitted by a single Boltzmann distribution function, the best-fit values for $\overline{V}$, k, and q_{max}/c_m were −44.3 mV, 7.5 mV, and 10.6 nC/μF for the second fiber and −39.1 mV, 11.2 mV, and 16.6 nC/μF for the third fiber.

After the addition of 20 mM creatine phosphate to the end pool solution, ~60 min were allowed for equilibration. The concentration of creatine phosphate in the myoplasm of the center pool region should be close to 20 mM. I_γ humps appeared in the ON segments of TEST minus CONTROL current traces in both experiments. The Q-V plots could be fitted very well by a sum of two Boltzmann distribution functions. The best-fit values for $\overline{V}_\beta$, k_β, $q_{\beta,max}/c_m$, $\overline{V}_\gamma$, k_γ, and $q_{\gamma,max}/c_m$ are −41.1 mV, 9.7 mV, 10.4 nC/μF, −54.5 mV, 2.8 mV, and 4.8 nC/μF for the second fiber and −22.7 mV, 16.1 mV, 8.1 nC/μF, −49.0 mV, 4.7 mV, and 12.7 nC/μF for the third fiber. In the second fiber, the values of the Boltzmann parameters for the Q_β component are similar to those for the total charge before the addition of creatine phosphate, but the amount of Q_γ reprimed is less than the average amount in control fibers. In the third fiber, the amount of total charge in the absence of creatine phosphate is larger than the amount of Q_β in 20 mM creatine phosphate, as in the first fiber.

Following the procedure applied to the first experiment, difference current traces were obtained from TEST minus CONTROL current traces before and after the addition of creatine phosphate. For the second fiber, ON and OFF charges were equal in the difference traces, within experimental error, whereas for the third fiber, ON charge was larger than OFF charge as in Fig. 6 *B*. The difference Q-V plots of OFF charge were fitted by a single Boltzmann distribution function. The plot of the second fiber is sigmoidal and the values of $\overline{V}$, k, and q_{max}/c_m are −57.3 mV, 4.0 mV, and 6.5 nC/μF. The plot of the third fiber is bell shaped and the values of the parameters are −48.0 mV, 3.2 mV, and 5.8 nC/μF. The value of q_{max}/c_m for the difference charge is larger (smaller) than the value of $q_{\gamma,max}/c_m$ in the presence of creatine phosphate in the second (third) fiber.

Results in this section show that when creatine phosphate was removed from the end pool solution, the I_γ hump disappeared. Comparison of Q-V plots before and after solution change and of difference Q-V plot suggests qualitatively that the disappearance of I_γ hump is not primarily due to a change in the time course of I_γ, but to an actual suppression of Q_γ as well. This indicates that creatine phosphate is required in the end pool solution for the maintenance of Q_γ. Removal of creatine phosphate from the end pool solution also has the secondary effect of increasing I_β or altering the waveform of the residual I_γ. The dose dependencies of these effects have not been studied.

Effect of Addition of External Cd^{2+}

When a depolarizing pulse of sufficiently large magnitude is applied to a muscle fiber, many ionic channels, including Ca channels, are opened. The slow inward Ca current makes the ON segment baseline in a TEST minus CONTROL current trace

deviate from a straight line. Also, the channels do not close instantaneously after the pulse. The decaying ionic current contaminates the OFF transient, as described by Horowicz and Schneider (1981). The potential at which the OFF charge begins to exceed the ON charge varies from fiber to fiber, but in our hands is usually > -30 mV. One way to reduce the inward Ca current is to add Cd^{2+} to the center pool solution (Cota et al., 1983; Donaldson and Beam, 1983).

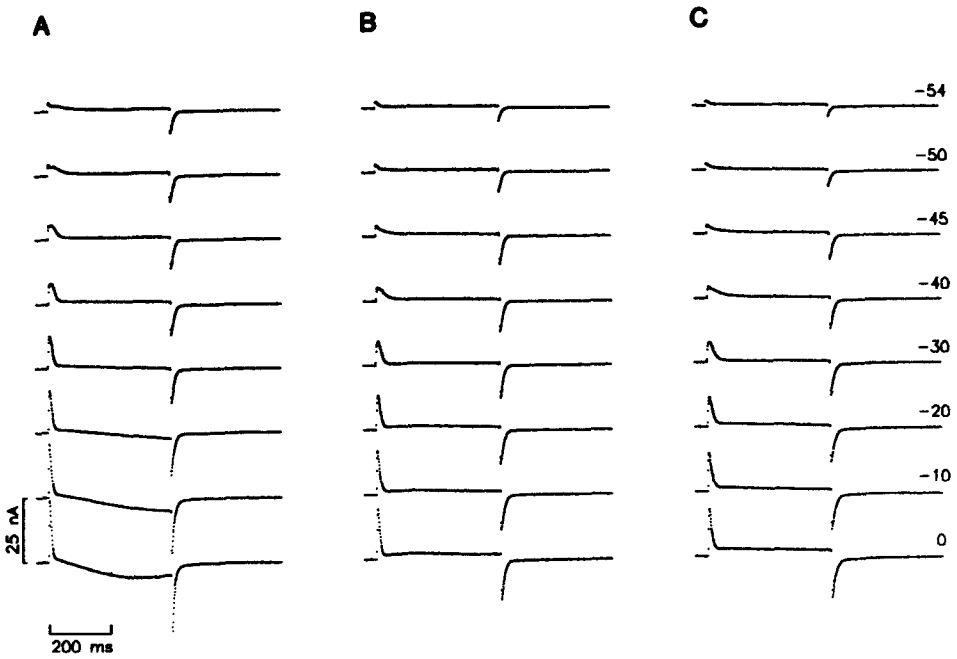

FIGURE 7. Effect of extracellular Cd^{2+} on TEST minus CONTROL currents in a cut fiber. Fiber identification: 87081. Diameter, 93 μm. Saponin treatment was applied to membrane segments in both end pools at time zero. After rinsing, the solutions in the end pools were replaced by solution B. Then, the solution in the center pool was changed to a TEA.Cl solution (solution E). At the 21st minute, the voltage clamp was turned on and the holding potential was set at -90 mV. From the beginning to the end of the experiment the holding current changed from -35 to -47 nA and $r_e/(r_e + r_i)$ decreased from 0.985 to 0.981. (*A*) Traces taken without Cd^{2+} in the center pool solution from the 55th to the 74th minute. At the 108th minute, 0.5 mM Cd^{2+} was added to the center pool solution. (*B*) Traces taken from the 120th to the 139th minute. At the 172nd minute, the $[Cd^{2+}]$ in the center pool solution was changed to 1 mM. (*C*) Traces taken from the 181st to the 200th minute. Only representative traces are shown in each panel. The numbers at the right show the potentials during the TEST pulses (same pulse for the traces in each row).

The traces in Fig. 7 were taken when the center pool solution contained 0 (*A*), 0.5 (*B*), and 1 mM (*C*) Cd^{2+}. In the absence of Cd^{2+}, the inward Ca current becomes noticeable at -20 mV (sixth trace in Fig. 7 *A*), as reflected by the negative deflection in the later part of the ON segment, and increases progressively with increasing levels of depolarization. When 0.5 mM Cd^{2+} was added to the center pool solution, the

inward Ca current was blocked, flattening the baselines in the ON segments of the traces in Fig. 7 *B*. In other fibers in which inward Ca current had a larger magnitude, 0.5 mM Cd^{2+} was insufficient to block the current completely. In this fiber, 0.5 mM was sufficient and 1 mM did not bring about much more change. However, further increase of [Cd^{2+}] to 2 mM generally caused the baseline of the OFF segment to droop (not shown), making it very difficult to estimate the area of the OFF transients. Thus, 0.5–1 mM seems to be the optimal [Cd^{2+}] to block inward Ca current in our cut fibers.

Although Cd^{2+} is useful in suppressing the inward Ca current, it is not without effect on charge movement. In the absence of Cd^{2+}, the ON segments of the first two traces in Fig. 7 *A* clearly show an I_γ hump. At −45 and −40 mV, the peak of I_γ actually rises above the peak of I_β. At potentials > −40 mV, I_γ peaks very early and

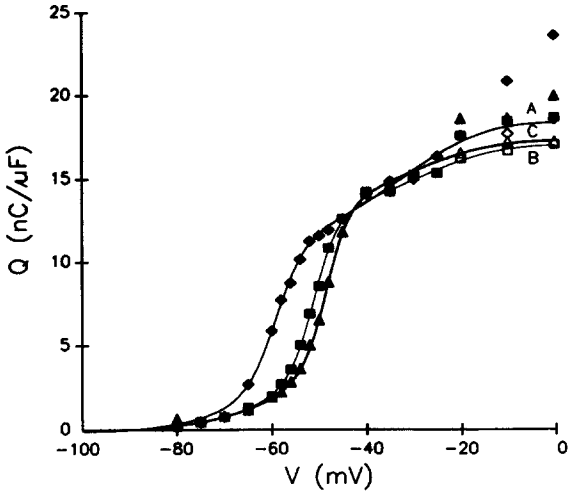

FIGURE 8. Steady-state voltage distributions of total charge in a cut fiber with different [Cd^{2+}] in the center pool solution. Same fiber as in Fig. 7. Diamonds show data taken with 0, squares with 0.5, and triangles with 1 mM Cd^{2+} in the center pool solution. Open symbols represent ON charge and filled symbols represent OFF charge. The points were obtained from the time integrals of ON or OFF transients in TEST minus CONTROL current traces, some of which are shown in Fig. 7. The smooth curves A–C were obtained by least-squares fits of a sum of two Boltzmann distribution functions to the three data sets. In each data set, ON charge was used for the fit when both ON and OFF charges are shown at the same potential; otherwise, OFF charge was used. The values of the best-fit parameters are given in Table V.

merges with the I_β component. Fig. 7 *B* shows that 0.5 mM Cd^{2+} made the I_γ humps in the first four traces much less prominent. At −30 mV, the peak of I_γ is above the shoulder in the rising phase, which presumably is the peak of I_β. This suggests that I_γ had not been completely suppressed, but its kinetics was slowed by 0.5 mM Cd^{2+}. This retarding effect was further magnified by 1 mM Cd^{2+} (traces in Fig. 7 *C*).

The amounts of ON or OFF charge with 0 (diamonds), 0.5 (squares), and 1 mM (triangles) Cd^{2+} are plotted as a function of TEST pulse potential in Fig. 8. Filled symbols represent OFF charge and open symbols represent ON charge. Undoubtedly, the difference between ON and OFF charges at −10 or 0 mV is reduced by Cd^{2+}. (At −20 mV, ON and OFF charges without Cd^{2+} overlap each other, which is probably due to scatter of the data). Unlike the situation with creatine phosphate removal, the steep portion in the *Q-V* plot was still present after the addition of 0.5 or

1 mM Cd^{2+}. Cd^{2+} simply shifted the plot to the right without affecting the total amount of charge appreciably. The three sets of data were well fitted by a sum of two Boltzmann distribution functions, represented by the smooth curves A–C. The best-fit parameters are listed in Table V under fiber 87081. In the presence of Cd^{2+}, $\overline{V}_\gamma$ was shifted to a less negative value and the value of $q_{\gamma,max}/c_m$ remained practically unchanged, confirming the presence of Q_γ. 1 mM Cd^{2+} did not appear to have much more effect than 0.5 mM Cd^{2+} in this fiber.

To understand why I_γ did not appear as a hump in the presence of Cd^{2+} while Q_γ apparently had not been abolished, each trace in Fig. 7 *B* was subtracted from the corresponding trace at the same potential in Fig. 7 *A* and the difference traces are shown in Fig. 9. At −54 mV, the ON transient of the difference trace is bell shaped. The amount of charge in the ON transient, listed in the legend, is equal to the

TABLE V

Effect of Cd^{2+} on Q-V Distributions of Q_β and Q_γ in Cut Fibers

(1) Fiber reference	(2) [Cd]	(3) c_m	(4) $\overline{V}_\beta$	(5) k_β	(6) $q_{\beta,max}/c_m$	(7) $\overline{V}_\gamma$	(8) k_γ	(9) $q_{\gamma,max}/c_m$
	mM	*μF/cm*	*mV*	*mV*	*nC/μF*	*mV*	*mV*	*nC/μF*
85061	0	0.142	−39.6	10.2	10.2	−49.1	2.9	13.7
	0.2	0.139	−39.9	10.4	9.6	−53.4	2.4	12.7
	0.4	0.139	−46.8	7.5	9.9	−53.4	2.4	11.3
	1.0	0.137	−43.8	7.0	10.0	−51.4	1.8	10.0
87011	0	0.109	−22.7	12.8	9.8	−50.4	4.9	18.4
	1.0	0.105	−35.7	13.9	11.6	−44.9	2.7	15.5
87081	0	0.137	−32.5	11.1	11.6	−60.4	3.1	12.5
	0.5	0.136	−29.7	11.3	7.5	−52.4	2.6	13.4
	1.0	0.133	−32.1	11.8	7.6	−49.8	2.5	13.4

Column 1 gives fiber identifications. Columns 2 and 3 give the [Cd^{2+}] in the center pool solution and the values of c_m, respectively. Columns 4–9 give the best-fit values of the parameters in the Boltzmann distribution functions of Q_β and Q_γ, with CONTROL charge correction and gap correction.

amount in the OFF transient, and these quantities represent the amount of Q_γ that disappeared at −54 mV in the presence of 0.5 mM Cd^{2+}. At −50 mV, the decay of the ON transient undershoots somewhat before returning to the baseline. This biphasic nature is more apparent in the ON segments of the bottom three traces. The net amounts of ON charge in these three difference traces are close to zero, suggesting that 0.5 mM Cd^{2+} did not suppress any Q_γ but slowed the kinetics of I_γ in this potential range. In contrast, the OFF segment in this potential range does not show much current transient, suggesting that the OFF current was not affected by the addition of Cd^{2+}. However, at higher levels of depolarization (not shown), the OFF segments of the difference traces show an inward transient, which is the ionic current blocked by 0.5 mM Cd^{2+}.

The difference in appearance between the first trace and the bottom three traces of Fig. 9 can be explained by the voltage shift of the $Q_\gamma - V$ curve by 0.5 mM Cd^{2+}. In

Fig. 8, Q_γ is close to saturation at −54 mV in curve A but slightly above threshold in curve B. The I_γ component in the first trace of Fig. 9 represents the current lost due to this voltage shift. At potentials ≥ −45 mV, Q_γ has reached saturation in both Q_γ–V curves. Hence, the difference traces reflect a change in the kinetics of I_γ during depolarization. As $\overline{V}_\gamma$ was shifted a few millivolts in the positive direction by 0.5 mM Cd^{2+}, it would be better to obtain the difference traces with a few millivolts offset between the traces in Fig. 7, *A* and *B*. However, such an offset might not be appropriate for the subtraction of I_β. Even with the shift, the I_γ components in the traces of Fig. 7 *B* still do not match those in the traces of Fig. 7 *A*.

Two other experiments were performed with varying [Cd^{2+}]. In both fibers, the I_γ hump was progressively slowed by increasing [Cd^{2+}]. The Q-V plots at different [Cd^{2+}]

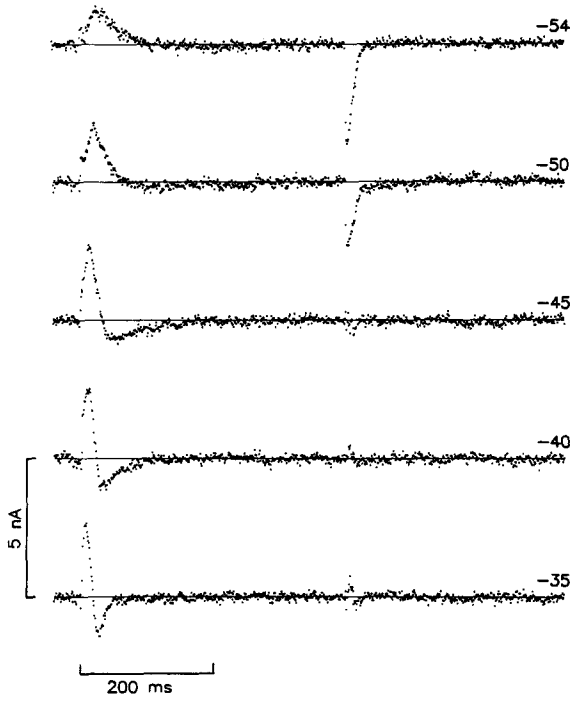

FIGURE 9. Difference traces of TEST minus CONTROL currents with and without 0.5 mM Cd^{2+}. Same fiber as in Fig. 7. Each trace was obtained by subtracting a trace in Fig. 7 *B* from the trace in the same row in Fig. 7 *A*. The amounts of ON/OFF charge in the five traces are 4.7/4.8, 4.2/4.2, −0.3/0.5, 0.0/0.2, and 0.0/0.0 nC/μF, respectively.

were fitted by a sum of two Boltzmann distribution functions. The best-fit parameters are listed in Table V. The parameters in each fiber were affected somewhat differently by Cd^{2+}. The positive shift of $\overline{V}_\gamma$ observed in the experiment of Fig. 8 was shared by only one of the two other fibers. Nonetheless, a common feature shared by all three fibers is that a substantial amount of Q_γ was present in 1 mM Cd^{2+}, although $q_{\gamma,max}/c_m$ was suppressed somewhat in two of the three fibers. Hence, the disappearance of the I_γ hump with Cd^{2+} in the center pool solution was not primarily due to a suppression of Q_γ, as in the case of removing creatine phosphate from the end pool solution, but rather to the prolongation of the time course of I_γ. (An alternative explanation will be given in the Discussion.) Just 0.5–1 mM Cd^{2+} is effective in

blocking inward Ca current, but this advantage is compromised by an alteration in the kinetics of I_γ.

When the experiments were performed, emphasis was put on obtaining the dose–response relationship of the effect of Cd^{2+} on charge movement and Ca current so as to gain information about the optimal [Cd^{2+}] to be used. No attempts were made to wash out the Cd^{2+} and bracket the control runs. Nonetheless, it is unlikely that the retardation of the kinetics of I_γ in the presence of Cd^{2+} was due to a rundown of the fibers, because at each [Cd^{2+}] two complete sequences of runs were taken. The shape of I_γ at each potential was the same in the two sequences. The time course of I_γ was prolonged at each potential only when the [Cd^{2+}] was increased. Recently we studied the effect of Co^{2+}, another Ca blocker, on charge movement. We focused on the reversibility of the effect of 20 mM Co^{2+} at the expense of the dose–response relationship. We found that this [Co^{2+}] also slowed the time course of I_γ and the effect was partially reversible (Hui, C.S., and W. Chen, unpublished results).

Effect of Maintained Hyperpolarization

In the measurements of charge movement and other electrophysiological signals, linear capacitive and ionic currents are routinely removed by subtracting a properly scaled CONTROL current taken in some subthreshold voltage range from the TEST current. If charge movement obeys the two-state Boltzmann distribution, some charge movement should exist in the CONTROL current trace and is inevitably subtracted from the TEST current trace. This problem can be minimized by setting the holding potential at 0 mV and taking CONTROL current traces in the positive potential range (Brum and Rios, 1987). However, with such a protocol, not too many CONTROL runs can be taken and one has to rely on interpolation to obtain a CONTROL current trace for every TEST current trace. Besides, if the fiber runs down at the end of the experiment, no reliable bracketing CONTROL current trace can be recorded. Moreover, there is worry about the physiological state of the fiber after maintained depolarization at 0 mV for an extended period of time. Another approach to minimize CONTROL charge is to set the holding potential at a highly negative level and take the CONTROL pulse in that potential range, but this results in an undesirably large holding current. Even a holding potential around −120 mV has some drawbacks for cut fibers mounted in a double Vaseline gap chamber as it affects the shape of the foot in the Q-V curve. This is explained by the theoretical curves shown in Fig. 10.

Curve A of Fig. 10 was generated by Eq. 2 in the preceding paper (Hui, 1991), with gap correction but without CONTROL charge correction, using the mean values of the Boltzmann parameters listed in Table II of that paper. As explained in detail in Fig. 2 of Hui and Chandler (1990), the finite and slowly rising foot of the curve is contributed by charge movement underneath the Vaseline seals. If CONTROL pulses are elicited from −110 to −90 mV, as in most of our cut fiber experiments, the CONTROL charge between these potentials is scaled up and subtracted from the TEST charge. The net charge measured at any potential is represented by curve C, which is given by the difference between curve A and straight line 1, which intersects curve A at −110 and −90 mV. However, if CONTROL pulses are elicited from −140

to −120 mV, the net charge measured at any potential is then represented by curve B, which is given by the difference between curve A and straight line 2, which intersects curve A at −140 and −120 mV. Thus, even without changing the holding potential and with the magnitude of the CONTROL pulse remaining constant, switching the CONTROL pulse potential to a more negative range alone would decrease the amount of CONTROL charge and increase the amount of charge moved at the same TEST potential. Without gap correction (e.g., if the resistance of the Vaseline seals is infinite), the slopes of lines 1 and 2 should be very close to zero and curves A–C should almost superimpose on each other.

In principle, subtraction of straight line 3, which intersects curve B at −110 and −90 mV, from curve B should also give curve C. In practice, the values of Q in a Q-V plot are normalized by c_m, which is estimated from the CONTROL current transient.

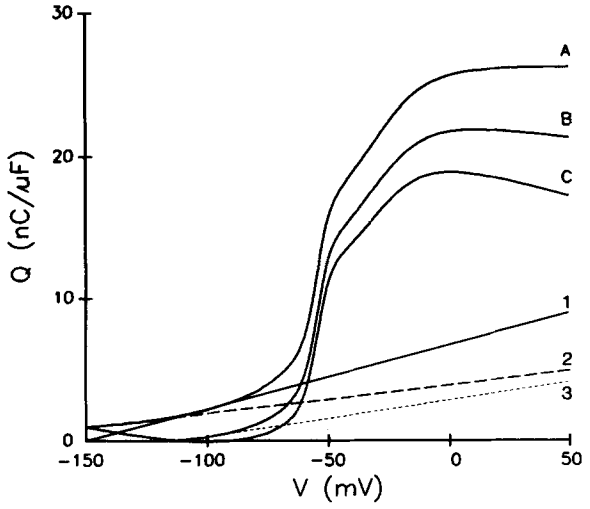

FIGURE 10. Theoretical Q-V curves describing the effect caused by a shift in CONTROL pulse potential. Curve A was generated according to a sum of two Boltzmann distribution functions, with gap correction, using the mean values of the parameters listed in Table II of the preceding paper (Hui, 1991). After correcting for CONTROL charge between −140 and −120 mV, the Q-V distribution is represented by curve B, which was obtained by subtracting line 2 from curve A. After correcting for CONTROL charge between −110 and −90 mV, the Q-V distribution is represented by curve C, which was obtained either by subtracting line 1 from curve A or by subtracting line 3 from curve B.

For CONTROL pulses from −110 to −90 mV (−140 to −120 mV), c_m is effectively measured at −100 mV (−130 mV). Since the voltage-dependent component of c_m at each potential is given by the first derivative of the Q-V plot, it is easy to visualize that the foot of the Q-V plot leads to a smaller value of c_m at −130 mV than its value at −100 mV (see Fig. 2 *C* of Hui and Chandler, 1990). Hence, subtraction of straight line 3 from curve B should yield a curve that is scaled up from curve C by a factor equal to $c_m(-100)/c_m(-130)$.

The above theoretical predictions explain some, but not all, of the effects when the holding potential was changed from −90 to −120 mV, as illustrated in the experiment of Fig. 11. *A* shows TEST minus CONTROL current traces taken when the holding potential was set at −90 mV and CONTROL pulses taken from −110 to

−90 mV. They look typical, with an I_γ hump clearly visible in the ON segments of the traces between −50 and −30 mV. After the holding potential was changed to −120 mV, CONTROL pulses were taken from −140 to −120 mV and the traces in *B* were recorded. The amplitudes of the ON and OFF transients were increased (note the change in vertical gain). At −50 and −44 mV, the I_γ hump disappears. At −40 mV,

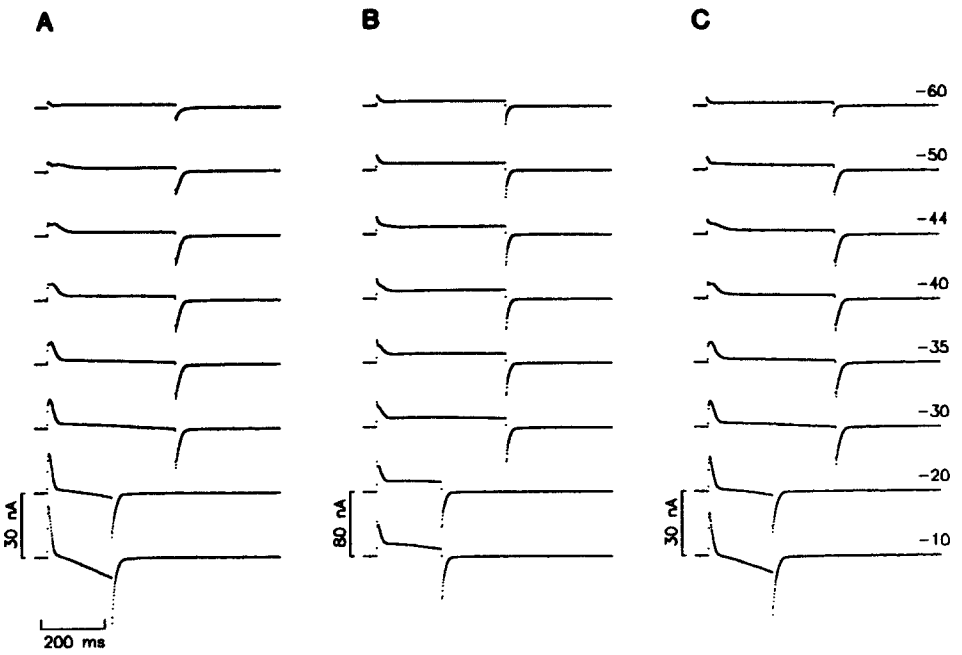

FIGURE 11. Effect of maintained hyperpolarization on TEST minus CONTROL currents in a cut fiber. Fiber identification: 83221. Diameter, 127 μm. Saponin treatment was applied to membrane segments in both end pools at time zero. After rinsing, the solutions in the end pools were replaced by Solution B. Then, the solution in the center pool was changed to a TEA.Cl solution (solution D). At the 24th minute, the voltage clamp was turned on and the holding potential was set at −90 mV. (*A*) Traces taken at −90 mV from the 68th to the 86th minute. At the 95th minute, the holding potential was changed to −120 mV. (*B*) Traces taken from the 100th to the 115th minute. At the 116th minute, the holding potential was restored to −90 mV. (*C*) Traces taken from the 120th to the 138th minute. The CONTROL pulses were always from 20 mV below the holding potential to the holding potential. Only representative traces are shown in each panel. The numbers at the right show the potentials during the TEST pulses (same pulse for the traces in each row). From the beginning to the end of the experiment, holding current changed from −22 to −32 nA and $r_e/(r_e + r_i)$ decreased from 0.993 to 0.991, except during maintained hyperpolarization, when they were −50 nA and 0.985, respectively.

the ON current decays with a fast and a slow exponential. The latter component could be I_γ but its shape is very different from that in the corresponding trace in *A*. At −35 and −30 mV, a small hump can be visualized in the decay phase of I_β. In addition, the positive pedestals in the ON segments of all the traces are greatly increased.

After the restoration of the holding potential to −90 mV, the traces in Fig. 11 *C* were taken. I_β and the maintained ionic currents returned to their original magnitudes but I_γ did not recover completely. At −50 and −44 mV, the I_γ humps in the ON segments are still smaller than the corresponding ones in Fig. 11 *A*. It is unlikely that this irreversibility of I_γ was due to a rundown of the fiber because control fibers without going through hyperpolarization generally showed little rundown in similar time periods.

The amounts of charge in the traces of Fig. 11 (and other traces not shown) are plotted against the TEST pulse potential in Fig. 12 *A* as diamonds (control −90 mV), squares (−120 mV), and triangles (bracketing −90 mV). Filled symbols represent OFF charge and open symbols represent ON charge. The three data sets were fitted by a sum of two Boltzmann distribution functions, represented by curves A–C. Curves A and C were corrected for CONTROL charge between −110 and −90 mV and curve B between −140 and −120 mV. As the holding potential was changed from −90 to −120 mV, the amount of charge in the foot and the maximum amount of charge were increased, as predicted by the theoretical curve B in Fig. 10, but both increases in Fig. 12 *A* are larger than the theoretical prediction. On returning to a holding potential of −90 mV, the changes were almost completely reversed.

The best-fit parameters of the three curves in Fig. 12 are listed in Table VI under fiber 83221. Comparison of the first and second rows of this entry shows that when the holding potential was changed from −90 to −120 mV, the value of $q_{\beta,max}/c_m$ was increased and $\overline{V}_\beta$ was shifted from −32 to −49 mV. This explains the drastic increase in the peak amplitude of I_β from the traces in Fig. 12 *A* to the corresponding traces in Fig. 12 *B*. The decrease in the value of c_m from 0.195 to 0.187 μF/cm can be explained by the shape of the foot of curve B in Fig. 12 *A*. A *Q-V* curve with gap correction but without CONTROL charge correction was generated with the parameters obtained for this fiber (listed in Table VI). The values of the voltage-dependent part of c_m at −90 and −120 mV were calculated from the tangents to the curve at these potentials and came out to be 0.0189 and 0.0075 μF/cm, respectively. Thus, the change in the slopes of the tangents is sufficient to account for the observed decrease in c_m. Two other similar experiments were performed and the results are included in Table VI. In all three fibers, k_β and $q_{\beta,max}/c_m$ were increased, $\overline{V}_\beta$ was shifted in the negative direction, and c_m was decreased when the holding potential was changed from −90 to −120 mV. In the two fibers in which the holding potential was returned to −90 mV, the above effects were mostly reversed.

According to the theoretical prediction shown in Fig. 10, if hyperpolarization has no other effect on charge movement, then curve B in Fig. 12 *A* can be converted to curve A by subtracting the scaled amount of charge between −110 and −90 mV, represented by the dashed straight line, and by scaling the resulting curve by $c_m(-100)/c_m(-130)$. This idea was tested as shown in Fig. 12 *B*. The diamonds and curve A in Fig. 12 *B* were replotted from Fig. 12 *A*, with the two filled diamonds at the largest depolarizations omitted. Filled squares in Fig. 12 *B* were calculated from the differences between the filled squares and the corresponding values on the dashed line in Fig. 12 *A*. Curve B in Fig. 12 *B* was obtained by fitting a sum of two Boltzmann distribution functions to the squares. The best-fit values for $\overline{V}_\beta$, k_β, $q_{\beta,max}/c_m$, $\overline{V}_\gamma$, k_γ, and $q_{\gamma,max}/c_m$ are −45.5 mV, 11.5 mV, 17.8 nC/μF, −59.3 mV, 4.6 mV,

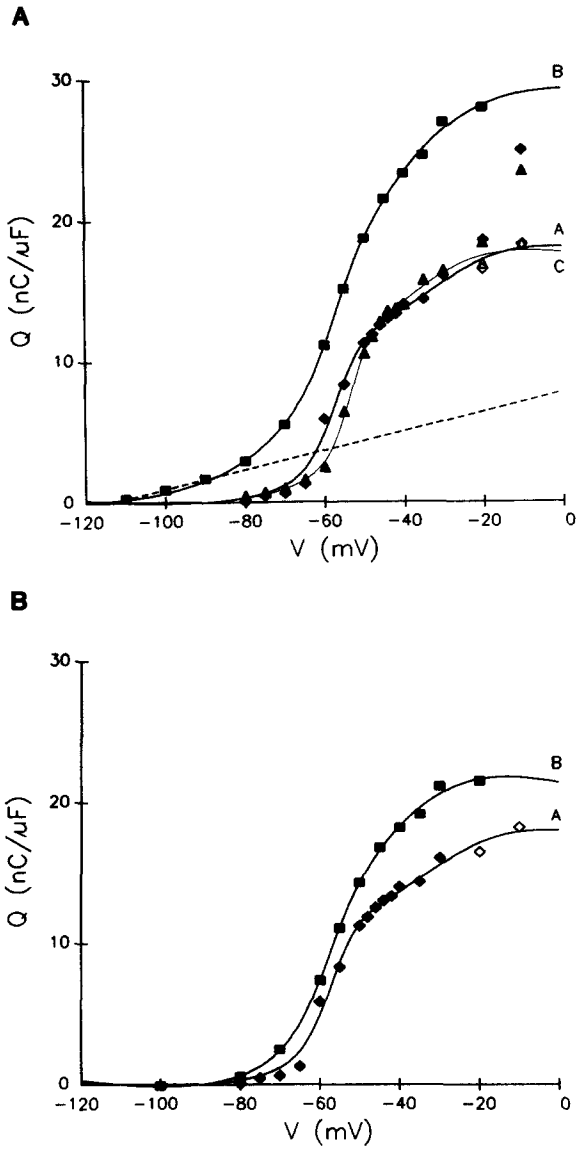

FIGURE 12. Steady-state voltage distributions of total charge in a cut fiber held at −90 or −120 mV. Same fiber as in Fig. 11. (*A*) Diamonds show data taken with the holding potential at −90 mV (control), squares at −120 mV, and triangles at −90 mV (bracketing). Open symbols represent ON charge and filled symbols represent OFF charge. The points were obtained from the time integrals of ON or OFF transients in TEST minus CONTROL current traces, some of which are shown in Fig. 11. The smooth curves A–C were obtained by least-squares fits of a sum of two Boltzmann distribution functions to the three data sets. In each data set, ON charge was used for the fit when both ON and OFF charges are shown at the same potential; otherwise, OFF charge was used. The values of the best-fit parameters are given in Table VI. The dashed line connects the two squares at −110 and −90 mV and is extrapolated in the positive direction. (*B*) The diamonds and curve A are replotted from *A*. Squares were obtained by subtracting the amounts of charge on the dashed line from the squares in *A*. Curve B was obtained by a least-squares fit of a sum of two Boltzmann distribution functions to the squares.

and 12.3 nC/μF. The values for Q_γ are similar in curves A and B, but $q_{\beta,max}/c_m$ is still larger and $\overline{V}_\beta$ is still 14 mV more negative in curve B than in curve A. As explained above with Fig. 10, part of the difference in $q_{\beta,max}/c_m$ can be explained by a difference in c_m. After multiplying $q_{\beta,max}/c_m$ by c_m from column 3 of Table VI, $q_{\beta,max}$ became 1.93 nC/cm for curve A and 3.33 nC/cm for curve B, which are still different. Possible explanations for the remaining difference will be given in the Discussion.

The main finding in this section is that, during maintained hyperpolarization to

−120 mV, I_γ was not manifested as a prominent hump due to an increase in the amplitude of I_β, reminiscent of the effect of replacing external Cl^- with SO_4^{2-}. However, with SO_4^{2-} the increase in the amplitude of I_β was caused by a large increase in $q_{\beta,max}/c_m$ together with a positive shift in $\overline{V}_\beta$, whereas, for maintained hyperpolarization, it was caused by a smaller increase in $q_{\beta,max}/c_m$ together with a negative shift in $\overline{V}_\beta$.

Effect of Repetitive Stimulation

It has always been of concern how frequently a cell can be stimulated without noticeably affecting a physiological signal. In charge movement experiments, a higher stimulation rate is desirable because it allows more traces to be recorded within a certain time period. With the present apparatus and protocol for measuring

TABLE VI

Effect of Maintained Hyperpolarization on Q-V Distributions of Q_β and Q_γ in Cut Fibers

(1) Fiber reference	(2) Holding potential	(3) c_m	(4) $\overline{V}_\beta$	(5) k_β	(6) $q_{\beta,max}/c_m$	(7) $\overline{V}_\gamma$	(8) k_γ	(9) $q_{\gamma,max}/c_m$
	mV	*μF/cm*	*mV*	*mV*	*nC/μF*	*mV*	*mV*	*nC/μF*
83211	−90	0.192	−24.8	12.3	10.9	−53.3	4.4	19.0
	−120	0.182	−36.5	21.0	28.7	−55.7	4.6	17.1
83221	−90	0.195	−31.7	9.9	9.9	−57.8	3.5	12.9
	−120	0.187	−48.5	13.6	24.2	−58.7	4.0	9.9
	−90	0.191	−36.9	9.1	9.6	−54.7	2.8	12.3
83282	−90	0.182	−25.7	11.1	7.5	−57.7	2.8	12.7
	−120	0.175	−45.4	17.8	17.3	−61.3	1.8	13.6
	−90	0.184	−39.7	11.7	10.5	−60.6	1.6	8.3

Column 1 gives fiber identifications. Columns 2 and 3 give the values of the holding potential and c_m, respectively. Columns 4–9 give the best-fit values of the parameters in the Boltzmann distribution functions of Q_β and Q_γ, with CONTROL charge correction and gap correction.

charge movement in cut fibers, single sweep TEST traces can be recorded that are relatively free of noise, eliminating the necessity for signal averaging. Hence, TEST minus CONTROL current traces can be recorded at a much faster rate than in intact fibers. However, the experiment shown in Fig. 13 alerts some caution against fast stimulation rates.

All the traces in the figure were elicited by a TEST pulse to −40 mV. The ON segment of the first trace shows a distinct I_γ hump having a peak as high as that of I_β and a time-to-peak of ~17 ms. The hump in the second trace, taken 1 min later, becomes less prominent. Its time-to-peak is prolonged to ~21 ms and its peak amplitude is reduced. The third trace, taken another minute later, is similar to the second. After a 13-min rest, the fourth trace shows an I_γ hump almost identical to that in the first trace, with the same time-to-peak. The bottom trace shows that after a 5-min rest the shape of the hump is still altered, with a time-to-peak of ~19 ms.

Although the shapes of the I_γ humps in the second, third, and fifth traces are different from those in the first and fourth traces, the amounts of ON or OFF charge are not different (see legend of Fig. 13). The difference trace (not shown) obtained by subtracting the second trace from the first trace showed a biphasic ON transient and a flat OFF segment, similar to the bottom three traces in Fig. 9. These suggest that when the I_γ hump became less prominent as a result of incomplete recovery after stimulation, it was not suppressed but was prolonged in time course. This fiber represents an extreme case in which the shape of I_γ did not recover fully even after a 5-min rest, and is chosen for the figure to emphasize the point. In most of the cut

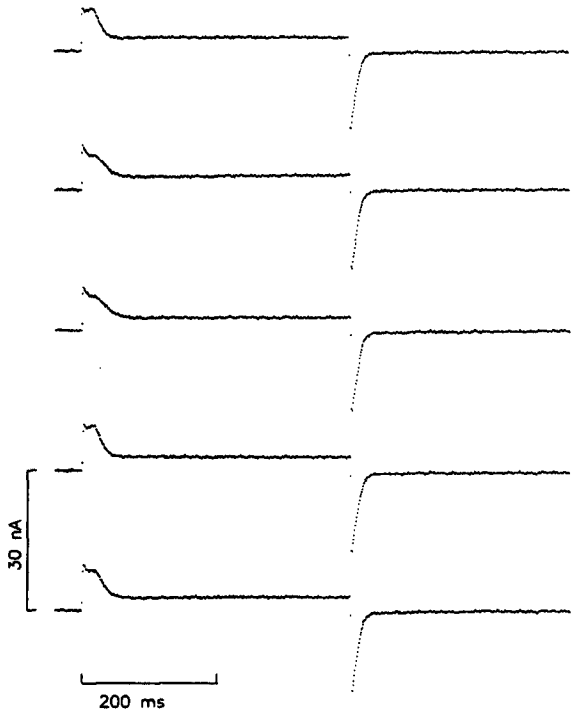

FIGURE 13. Effect of the rate of stimulation on TEST minus CONTROL currents in a cut fiber. Fiber identification: 7D081. Diameter, 119 μm. Saponin treatment was applied to membrane segments in both end pools at time zero. After rinsing, the solutions in the end pools were replaced by solution B. Then the solution in the center pool was changed to a TEA.Cl solution (solution D). At the 24th minute, the voltage clamp was turned on and the holding potential was set at −90 mV. The traces were elicited by a TEST pulse to −40 mV at the 55th, 56th, 57th, 70th, and 75th minutes. In that period, the holding current and $r_e/(r_e + r_i)$ remained constant at −41 nA and 0.985. The amounts of ON/OFF charge in the five traces are 12.2/13.1, 13.1/13.1, 13.1/12.9, 13.4/13.3, and 14.1/13.6 nC/μF, respectively.

fibers studied, the shape of I_γ recovered almost completely in 1 min. However, if the stimulation rate is faster than once per minute, the recovery might not be complete, depending on the condition of the fiber.

DISCUSSION

Several manipulations resulted in the disappearance of the I_γ hump in TEST minus CONTROL current traces, but the underlying causes for the disappearance were different. Replacement of extracellular Cl^- by SO_4^{2-} caused the disappearance by an increase in I_β (Hui and Chandler, 1990) and lowering the temperature from 14 to 6°C

caused the disappearance by prolonging the time course of I_γ (Hui, 1991). This paper describes five additional manipulations that affected the appearance of I_γ. Replacement of extracellular Cl^- by $MeSO_3^-$ caused a negative shift of the voltage dependence of I_γ kinetics, but prominent I_γ humps could still be observed in the TEA.$MeSO_3$ solution. Removal of creatine phosphate from the end pool solution suppressed the I_γ hump by reducing the amount of Q_γ. Maintained hyperpolarization resulted in an increase in I_β, thereby obscuring the I_γ hump, similar to the effect of SO_4^{2-}. Addition of Cd^{2+} to the center pool solution and repetitive stimulation prolonged the time course of I_γ such that I_γ was not manifested as a prominent hump, similar to the effect of cooling. I_γ was originally defined as the delayed hump component in the ON segment of a TEST minus CONTROL current trace (Adrian and Peres, 1979; Hui, 1991). This definition only holds when I_γ is manifested as a hump but loses its meaning when I_γ has a much broader time course. In the latter case, I_γ should be identified with the current generated by the flow of the steeply voltage-dependent charge component.

Among the five manipulations studied in this paper, $MeSO_3^-$ has the least effect on the appearance of the I_γ hump. In fact, after allowing for the negative voltage shift, the kinetics of I_γ might not be different in the TEA.Cl and TEA.$MeSO_3$ solutions. Table III shows that the fraction of Q_γ in the total charge was the same in both solutions. In contrast, the amount of Q_β was greatly increased when Cl^- was replaced by SO_4^{2-}, reducing the fraction of Q_γ in the total charge from one-half to one-fourth (Hui and Chandler, 1990). Hence, to visualize I_γ as a hump, $MeSO_3^-$ is a better substitute for Cl^- than SO_4^{2-}. It is also worth noting that the negative (positive) shift in $\overline{V}_\gamma$, when Cl^- is replaced by $MeSO_3^-$ (SO_4^{2-}), is parallel to the negative (positive) shift in contraction threshold (Kao and Stanfield, 1968; Foulks and Perry, 1977).

We have investigated other anion substitutes for Cl^- and they all affected charge movement to some extent. To our surprise, gluconate greatly suppressed Q_β (Chen and Hui, 1991*b*), opposite to the effect of SO_4^{2-}. Thus, gluconate would be a better substitute for Cl^- if one wants to study Q_γ exclusively.

It is possible that the appearance of I_γ might depend on other factors, such as the species of frog (*Rana temporaria* vs. *Rana pipiens* or *Rana catesbiana*), the source of supply (Northern vs. Southern *Rana pipiens*), the season of the shipment, the mode of adaptation (warm vs. cold), and the mode of feeding. In this series of papers, *Rana temporaria* were used and they were always cold-adapted for at least a week before experimentation.

Possible Origin of I_β and I_γ

In the parallel model of charge movement (Hui and Chandler, 1990), Q_β and Q_γ are considered as two separate species of charge moving independently. An alternative view is that both Q_β and Q_γ belong to the same charge species. Q_β triggers Ca release, which in turn induces the movement of more charge (i.e. Q_γ [Csernoch et al., 1989; Pizarro et al., 1990]). Both models can explain some of the results in this paper. Recently we experienced some cut fibers having a usual amount of Q_γ but very little Q_β (Chen and Hui, 1991*a*). This finding is consistent with the parallel model in which Q_γ can move irrespective of the presence of Q_β. We are thus tempted to speculate that

Q_γ plays the role of triggering Ca release, although it remains to be demonstrated that the fibers with little Q_β can release normal amount of Ca.

A molecular mechanism was proposed in the preceding paper (Hui, 1991) to explain the complicated kinetics of I_γ. Chen and Hui (1990) reported that nifedipine suppressed both Q_β and Q_γ. The tetramers of dihydropyridine binding proteins might indeed provide the charge movement that is observed as I_γ, but the origin of I_β still remains open. It is quite likely that I_β consists of several components, including sodium channel gating current, potassium channel gating current, Ca channel gating current, and charge movement that has no known physiological function yet. It is also possible that the movement of charge in the monomeric form of the dihydropyridine binding protein contributes to I_β. This latter component is speculative, but it accommodates any interconversion between Q_β and Q_γ, as was suggested by the experiments studying the effect of creatine phosphate in the internal solution. It is premature to speculate that an interconversion between Q_β and Q_γ occurred. Nonetheless, in another group of experiments there was an indication that perchlorate might increase the amount of Q_γ at the expense of Q_β (Hui, C.S., and W. Chen, unpublished results).

Effects of the Interventions on I_β and I_γ

Part of the increase in charge movement during maintained hyperpolarization in cut fibers is a consequence of the enhancement of the foot of the *Q-V* curve contributed by the charge in the membranes underneath the Vaseline seals (Hui and Chandler, 1990). This characteristic does not apply to intact fibers, but is inevitable in cut fibers unless the resistance of the seals could be made infinite. After correcting for the charge movement between −110 and −90 mV, $q_{\beta,max}/c_m$ of curve B in Fig. 12 *B* is still larger than that of curve A. Part of the remaining difference is due to a decrease in c_m at −120 mV. Although a decrease in Q_2 at −120 mV (Brum and Rios, 1987) could explain this decrease in c_m, the change in slope at the foot of curve B in Fig. 12 *A* is sufficient to explain the decrease, as described in the Results. After correcting for the difference in c_m, the value of $q_{\beta,max}$ for curve B of Fig. 12 *B* is still larger than that for curve A. Again, this final difference could be explained by a decrease of Q_2 at −120 mV (Brum and Rios, 1987). Alternatively, if Q_β indeed consists of several components as speculated above, it is possible that hyperpolarization reprimes one or more components that have a more negative voltage distribution relative to those of the other components. Although the cause of the increase in Q_β is not understood, the experiments in this paper clearly show that maintained hyperpolarization to −120 mV obscures the appearance of the I_γ hump by an increase in I_β. If the effect is graded, maintained hyperpolarization to −100 or −110 mV would still obscure the hump, although to a lesser extent.

Cd^{2+} was found to slow the kinetics of I_γ. If I_γ is caused by Ca release, then the slowing of the kinetics of I_γ could be related to the slowing of the kinetics of Ca release by Cd^{2+}. On the other hand, if Ca release is triggered by Q_γ, it is equally likely that the slowing of the kinetics of Ca release is due to the slowing of the triggering mechanism. To pin down which alternative is correct, it is important to find out whether Q_γ is the cause or the consequence of Ca release. For the present moment, caution should be taken in using Cd^{2+} to block Ca current if the kinetics of charge

movement or Ca release is under study. Co^{2+} has similar effect on the kinetics of I_γ (Hui, C.S., and W. Chen, unpublished results). It may be possible to find a Ca channel blocker that does not have this effect. More experiments are required to achieve this goal.

Repetitive stimulation also slowed the kinetics of I_γ. In the extreme case shown in Fig. 13, the I_γ hump did not recover fully even after a 5-min rest. In general, the recovery time depends on the condition of the fiber and the experimental conditions. In our hands, one stimulation per minute is considered as optimal. Results of experiments by Schneider et al. (1987) suggested that the SR could be depleted of Ca^{2+} after a conditioning TEST pulse when [EGTA] in the internal solution was only 0.1 mM. Garcia et al. (1989) also observed a substantial depletion of Ca^{2+} in the SR by repetitive stimulation at 0.03 Hz when [EGTA] in the internal solution was 1 mM. Since the experiments in this paper were performed with 20 mM EGTA in the internal solution, the SR should be depleted of Ca^{2+} more readily than with lower [EGTA]. However, in a healthy cut fiber prominent I_γ humps could be observed for as long as 6 h. Thus, superficially, one might conclude that I_γ could not arise as a consequence of Ca release. On the other hand, I_γ could still be the trigger for Ca release because the trigger can be unaffected even when the SR is depleted of Ca^{2+}.

This conclusion can be challenged by arguing that the apparent depletion of Ca^{2+} in the SR was based on the Ca–dye signal recorded globally from the myoplasm of many sarcomeres. If the $[Ca^{2+}]$ in the restricted region between the tubular membrane and the junctional SR membrane is high after Ca release, I_γ humps can still be observed. To chelate the Ca^{2+} in the putative restricted region, Garcia et al. (1990) raised the [EGTA] in the internal solution to 62.5 mM and observed a parallel suppression of the I_γ hump and the intrinsic optical signal that is thought to reflect Ca release. The result does not necessarily prove that the I_γ hump is the consequence of Ca release, because in the presence of such high [EGTA] the trigger for Ca release might not be in a normal state after the first activation. A perturbation on the recovery of the trigger could lead to a parallel perturbation on the recovery of the release. In addition, we have studied the effect of repetitive stimulations on the I_γ hump in the presence of 50 mM EGTA in the end pool solution. The fibers were stimulated by a train of up to 10 identical TEST pulses at a rate of once per 6 s. In the usual potential range, very pronounced I_γ humps could still be observed during the last TEST pulse (Hui, C.S., and W. Chen, unpublished results), different from the finding of Garcia et al. (1990). Although pronounced I_γ humps were present in the later runs of the train, the shape of the hump in the second run was somewhat different from that in the first run, suggesting that the I_γ hump might not have completely recovered after 6 s. It is still preferable to perform experiments at a stimulation rate of once per minute.

Hence, the exceptionally slow recovery of the shape of the I_γ hump in Fig. 13 was probably related to the condition of the fiber. Although this extreme case is very rare, it alerts us that the I_γ hump might take a longer time to recover in some fibers than others.

The slow recovery of I_γ kinetics in cut fibers after stimulation has not been observed in intact fibers. To acquire charge movement traces signal-averaged 8 or 16 times, intact fibers were generally stimulated at rates faster than once per minute; otherwise,

there might not be enough time to complete the experiment. At such a fast rate, there was no noticeable change in the shape of I_γ between successive traces (unpublished observations). This adds another item to the list of differences between the two preparations.

The author would like to thank Drs. Steve Baylor, Knox Chandler, Judith Heiny, and Eduardo Rios for reading the manuscript, Dr. Fred Sigworth and the staff of Yale Electronics Lab for designing and fabricating the voltage clamp module and interface card for laserjet printer, and Dr. Siu Hui for expert advice on statistics.

This project was supported by grants from the National Institutes of Health (NS-21955), the Muscular Dystrophy Association, and the American Heart Association. The author was a recipient of a Research Career Development Award (NS-00976) from the NIH.

Original version received 30 March 1990 and accepted version received 15 January 1991.

REFERENCES

Adrian, R. H., and A. R. Peres. 1979. Charge movement and membrane capacity in frog muscle. *Journal of Physiology.* 289:83–97.

Brum, G., and E. Rios. 1987. Intramembrane charge movement in frog skeletal muscle fibres: properties of charge 2. *Journal of Physiology.* 387:489–517.

Chandler, W. K., and C. S. Hui. 1990. Membrane capacitance in frog cut twitch fibers mounted in a double Vaseline-gap chamber. *Journal of General Physiology.* 96:225–256.

Chen, W., and C. S. Hui. 1990. Differential blockage of Q_β and Q_γ by nifedipine in frog cut twitch fibers. *Biophysical Journal.* 57:169*a*. (Abstr.)

Chen, W., and C. S. Hui. 1991*a*. Existence of Q_γ in frog cut twitch fibers with little Q_β. *Biophysical Journal.* 59:503–507.

Chen, W., and C. S. Hui. 1991*b*. Gluconate suppresses Q_β more effectively than Q_γ in frog cut twitch fibers. *Biophysical Journal.* 59:543*a*. (Abstr.)

Cota, G., L. Nicola Siri, and E. Stefani. 1983. Calcium-channel gating in frog skeletal muscle membrane: effect of temperature. *Journal of Physiology.* 338:395–412.

Crank, J. 1956. The Mathematics of Diffusion. Clarendon Press, Oxford.

Csernoch, L., I. Uribe, M. Rodriguez, G. Pizzaro, and E. Rios. 1989. Q_γ and Ca release flux in skeletal muscle fibers. *Biophysical Journal.* 55:88*a*. (Abstr.)

Donaldson, P. L., and K. G. Beam. 1983. Calcium currents in fast twitch skeletal muscle of the rat. *Journal of General Physiology.* 82:449–468.

Foulks, J. G., and F. A. Perry. 1977. Some effects of organic anions on excitability and excitation-contraction coupling in frog skeletal muscle. *Canadian Journal of Physiology and Pharmacology.* 55:700–708.

Garcia, J., M. Amador, and E. Stefani. 1989. Relationship between myoplasmic calcium transients and calcium currents in frog skeletal muscle. *Journal of General Physiology.* 94:973–986.

Garcia, J., G. Pizarro, E. Rios, and E. Stefani. 1990. Depletion of the SR reduces the delayed charge movement of frog skeletal muscle. *Biophysical Journal.* 57:341*a*. (Abstr.)

Godt, R. E., and D. W. Maughan. 1988. On the composition of the cytosol of relaxed skeletal muscle of the frog. *American Journal of Physiology.* 254:C591–604.

Hodgkin, A. L., and P. Horowicz. 1959. The influence of potassium and chloride ions on the membrane potential of single muscle fibres. *Journal of Physiology.* 148:127–160.

Horowicz, P., and M. F. Schneider. 1981. Membrane charge movement in contracting and non-contracting skeletal muscle fibres. *Journal of Physiology.* 314:565–593.

Huang, C. L.-H. 1982. Pharmacological separation of charge movement components in frog skeletal muscle. *Journal of Physiology.* 324:375–387.

Hui, C. S. 1983*a*. Pharmacological studies of charge movement in frog skeletal muscle. *Journal of Physiology.* 337:509–529.

Hui, C. S. 1983*b*. Differential properties of two charge components in frog skeletal muscle. *Journal of Physiology.* 337:531–552.

Hui, C. S. 1991. Comparison of charge movement components in intact and cut twitch fibers of the frog. Effects of stretch and temperature. *Journal of General Physiology.* 98:287–314.

Hui, C. S., and W. K. Chandler. 1990. Intramembranous charge movement in frog cut twitch fibers mounted in a double Vaseline-gap chamber. *Journal of General Physiology.* 96:257–297.

Hui, C. S., and W. K. Chandler. 1991. Comparison of Q_β and Q_γ charge movement in frog cut twitch fibers. *Journal of General Physiology.* In press.

Hutter, O. F., and D. Noble. 1960. The chloride conductance of frog skeletal muscle. *Journal of Physiology.* 151:89–102.

Kao, C. Y., and P. R. Stanfield. 1968. Actions of some anions on electrical properties and mechanical threshold of frog twitch muscle. *Journal of Physiology.* 198:291–309.

Melzer, W., M. F. Schneider, B. J. Simon, and G. Szucs. 1986. Intramembrane charge movement and calcium release in frog skeletal muscle. *Journal of Physiology.* 373:481–511.

Pizarro, G., M. Rodriguez, L. Csernoch, and E. Rios. 1990. Positive feedback in skeletal muscle E-C coupling. *Biophysical Journal.* 57:401*a*. (Abstr.)

Schneider, M. F., B. J. Simon, and G. Szucs. 1987. Depletion of calcium from the sarcoplasmic reticulum during calcium release in frog skeletal muscle. *Journal of Physiology.* 392:167–192.

Vergara, J., and C. Caputo. 1983. Effects of tetracaine on charge movements and calcium signals in frog skeletal muscle fibers. *Proceedings of the National Academy of Sciences, USA.* 80:1477–1481.